

A search for cool molecular gas in GK Persei and other classical novae

Tomek Kamiński¹, Helena J. Mazurek², Karl M. Menten³, and Romuald Tylenda¹

¹ Nicolaus Copernicus Astronomical Center, Polish Academy of Sciences, Rabiańska 8, 87-100 Toruń, e-mail: tomkam@ncac.torun.pl

² Institute of Astronomy, Nicolaus Copernicus University, Grudziądzka 5, 87-100 Toruń, Poland

³ Max-Planck-Institut für Radioastronomie, Auf dem Hügel 69, 53-121 Bonn, Germany

January 26, 2022

ABSTRACT

Detecting molecular line emission from classical nova remnants has the potential of revealing information on the composition of the ejecta, in particular, it can deliver accurate isotopic ratios in the matter processed by a thermonuclear runaway. We conducted searches toward more than 100 classical novae for emission in lines of the CO or HCN molecules using single-dish telescopes and interferometric arrays at millimeter and submillimeter wavelengths. The survey demonstrates that classical novae, young or old, are not strong sources of molecular emission at submillimeter and millimeter wavelengths. Additionally, we mapped CO emission around Nova Persei 1901 (GK Per), earlier claimed to be circumstellar in origin. Our measurements indicate that the observed emission is from the interstellar medium. Although no molecular emission at millimeter and submillimeter wavelengths has been found in classical novae, it is still likely that some will be detected with high-sensitivity interferometers such as ALMA.

Key words. surveys – stars: novae, cataclysmic variables – circumstellar matter – stars: individual: GK Per, V1148 Sgr

1. Introduction

Classical novae are close binary systems where a white dwarf accretes material from a companion, typically a late-type dwarf. Accretion via a disk accumulates hydrogen in a degenerate layer on the surface of the white dwarf (Warner 1995; Bode & Evans 2008). At some point, the pressure and temperature at the bottom of the accreted envelope become high enough for hydrogen burning to start. This initiates the thermonuclear runaway process that is directly responsible for classical novae outbursts at luminosities of 10^4 – $10^5 L_{\odot}$. The energetic explosion on the surface of a white dwarf ejects the accumulated material, and, according to some models, may even remove some material forming the outer layers of the white dwarf. A typical mass lost during a single nova explosion is 10^{-7} – $10^{-3} M_{\odot}$. A few percent of this material was processed by the thermonuclear burning.

Although studied for decades, classical novae are still not fully understood. In particular, the physics of thermonuclear runaway and dust formation associated with novae remain unclear. It is very difficult to model the thermonuclear runaway, mainly because (1) we do not know the mechanism that mixes the accreted envelope and the outermost shells of the white dwarf; (2) we do not fully understand the process of material ejection; and (3) nuclear reaction rates are uncertain (Hix 2001). In consequence, it is not known how effective classical novae are in enhancing the ejected material with products of nuclear burning. Knowing the composition of classical novae ejecta is of great importance because the material eventually reaches the interstellar medium, enhancing it with the nuclear ashes. Classical novae are currently thought to be the major source of ^{13}C , ^{15}N , and ^{17}O in the Galaxy (Li et al. 2016; Romano & Matteucci 2003) and are likely to significantly contribute to the Galactic content of ^7Li , ^{19}F , and ^{26}Al (Gehrz et al. 1998; Izzo et al. 2015).

There is thus a great need for robust measurements of the composition of classical novae ejecta. The so-called presolar “nova grains”, should they indeed originate in classical novae outburst, provide only a limited and biased information on the ejecta composition (Amari et al. 2001; Iliadis et al. 2018). To date, only a handful of observations has been made whose results permit direct tests of theoretical predictions for the isotopic yields of nova thermonuclear runaway. There is thus a great need for observational data from which elemental isotopic abundances could be inferred (e.g. Black 2005) and compared to models. Observational astronomy often relies on molecular spectra to constrain the isotopic composition of objects.

Molecules are expected to form in ejecta of classical novae (Pontefract & Rawlings 2004; Derdzinski et al. 2017). Observations collected in the last decades corroborate this notion. First, it is clear from observations that 30–40% of classical novae produce dust 10–100 days after their outbursts (Bode & Evans 2008). Dust cannot be produced without the presence of parent molecules or nucleation seeds, whose formation requires simple diatomic species. Furthermore, dust provides protection for the molecules from the Galactic ultraviolet (UV) field and from the harsh radiation of the nova explosion. Second, molecules are observed in spectra of classical novae at optical and near-infrared (NIR) wavelengths, including bands of C_2 , CN, and CO (e.g., Wilson & Merrill 1935; Nagashima et al. 2014; Banerjee et al. 2016; Fujii et al. 2021, and references therein). At these wavelengths, the isotopic shift between different isotopologs is typically too small to be resolved, owing to generally modest spectral resolutions and high intrinsic line widths (500 – 5000 km s^{-1}). The spectral confusion hampers stringent observational tests for nova nucleosynthesis. A straightforward method of measuring isotopic ratios, successfully applied to the envelopes of evolved stars and the interstellar medium, are ground-based observations

of molecular rotational transitions at millimeter (mm) and sub-millimeter (submm) wavelengths.

There have been attempts to detect mm-wave molecular emission in classical novae, which almost all (see Sect. 3) turned out to be unsuccessful or resulted in detections in ambient material unrelated to the nova phenomenon (for a review see Sect. 13 in Bode & Evans 2008). Past attempts resulted in upper limits on CO emission obtained with the Swedish-ESO Submillimeter Telescope (SEST) (Weight et al. 1993; Nielbock & Schmidtobreick 2003), the IRAM 30 m telescope (Shore & Braine 1992), and with the University of Texas Millimeter Wave Observatory (Albinson & Evans 1989). The reports from before ~ 1995 are however unreliable and often contradictory. The outflow velocities in novae are of $500\text{--}5000\text{ km s}^{-1}$ and are thus expected to have very broad lines, which require receivers with a broad bandwidth, and with flat and stable spectroscopic baselines, which in the past were difficult to attain. Most of the published negative results were obtained with instruments which did not fulfill these requirements. Some claims of nonexistent emission have been recently debunked. For instance, a lack of detection of CO(1–0) was reported for Nova 1670 (also known as CK Vul) by Weight et al. Observed in 2014–2015 with modern receiver systems, CK Vul showed clear emission lines of CO for $J_{\text{up}} < 7$ (Kamiński et al. 2015, 2017). However, CK Vul turned out to not be a classical nova but a red nova, that is a stellar merger product, although with similarly broad lines as expected for classical novae, that is $\approx 300\text{ km s}^{-1}$. Another example is η Carinae, which is not a nova but a luminous blue variable with broad lines. η Car was long claimed to be free of molecular mm-wave emission (e.g. Cox & Bronfman 1995). However, when observed with APEX/FLASH in 2011, it showed a plethora of molecular features (Loinard et al. 2012). Another example is the first observation of rotational lines of SiO and CO in the remnant of SN 1987A (Kamenetzky et al. 2013) using the ALMA interferometer. The lines of the supernova remnant are very broad, $\text{FWHM} \approx 2200\text{ km s}^{-1}$, but were recovered within the ALMA correlator bandwidth, even though the lines were broader than the covered spectral band. For classical novae, spectral lines can be as broad as a few GHz in the mm range, and one needs a receiver system with a large instantaneous bandwidth to be even able to recognize a line and to distinguish its presence from an elevated continuum level.

Encouraged by the discoveries in CK Vul, η Car, and SNR 1987A, we decided to revise the view on the presence of molecular emission in classical novae by undertaking an observation campaign aimed to detect molecules at mm wavelengths using modern instruments, including single-dish telescopes and interferometers. The search for molecular emission in the common isotopologs was meant as the first step towards providing isotopic ratios in thermonuclear ashes of classical novae. In Sect. 2.1 and 2.2, we present observations with APEX and IRAM 30 m telescopes for a large sample of classical novae and related objects. In Sect. 3, we revise the nature of molecular emission near nova remnant GK Per based on mapping observations from the IRAM telescope. In Sect. 4, we present our attempts to detect molecular emission with the SMA and ALMA interferometers. Finally, in Sect. 5 we summarize the observational material and conclude our findings.

2. Single-dish observations

In 2014–2016, we conducted surveys of old classical nova with the APEX and IRAM telescopes, targeting emission lines of CO and HCN in novae on both hemispheres. The idea was to observe

many sources at a sensitivity level comparable to that at which emission lines would be easily detectable in CK Vul. This typically required 5–20 min of integration on source. We searched for lowest rotational transitions of CO and HCN, because these are usually the strongest lines in cool circumstellar¹ envelopes. Particularly, emission of HCN might be expected to be strong if the gas is enhanced in CNO-processed material, as expected for classical novae.

The sources were selected from the *Central Bureau for Astronomical Telegrams (CBAT) List of Novae in the Milky Way*², which includes many historical novae. Individual targets were chosen for observations based on their availability during periods assigned to us at the observatories. The lists of sources observed with the APEX and the IRAM telescopes are given in Tables 1 and 2, respectively. There, we classified the observed objects using the SIMBAD astronomical database³ of Centre de Données Astronomiques de Strasbourg (CDS). According to this classification, as of August 2020, eleven of the observed sources are not novae despite being listed as such in the CBAT catalog. Twelve other objects are dwarf novae. We decided to include them in our survey summary nevertheless. Technical details on the observations are given below.

2.1. APEX observations and data reduction

The fifty-nine objects listed in Table 1 were observed with the Atacama Pathfinder Experiment (APEX) 12-m submillimeter telescope (Güsten et al. 2006). Forty-five of these objects are classified as classical novae. The observations took place in 24–28 July 2014, 4 April 2015, 8–11 June 2015, 10 July 2015, 30 July 2016, and 1, 6, 13 and 14 July 2016. For frequencies between 278 and 492 GHz, we used the FLASH⁺ receiver (Klein et al. 2014), which operated simultaneously in two atmospheric bands at about 345 GHz and 460 GHz. The version of FLASH⁺ separates the two heterodyne sidebands in each of its two modules, which cover the 345 and 460 GHz bands, giving four spectra, each 4 GHz wide. The image-band rejection factors used are all above 10 dB and at most frequencies the rejection is higher than 20 dB. In all APEX observations, we used the eXtended Fast Fourier Transform Spectrometer (XFFTS; Klein et al. 2012), which typically provided us with resolutions better than 0.05 km s^{-1} . To decrease the noise to levels appropriate for the expected broad lines, we rebinned the spectra to a much lower resolution, typically near 30 km s^{-1} . In all observations, we used wobbler switching with the maximal azimuthal wobbler throw of $300''$ (typically throws of $60\text{--}100''$ were used), which resulted in flat baselines.

Overall, with APEX we covered four spectral ranges characterized in Table 3. The table includes the nominal FWHM beam size and the main-beam efficiency (η_{mb}). In the two out of four units of FLASH⁺, we obtained spectra centered on the CO(3–2) and (4–3) lines with rest frequencies of 345.79598990 and 461.0407682 GHz, respectively. Also covered were the H¹³CO(4–3), SiS(19–18), and SiO(8–7), transition which are readily apparent in the spectrum of one of our the sources we observed to check the telescope’s pointing performance, that is IRC+10216 (cf. Fig. A.1). We also registered the upper side band spectra (which we refer to as ‘CO(3–2) OSB’ and ‘CO(4–3) OSB’). We present all results in the antenna (T_A^*) temperature

¹ By circumstellar we mean in this paper material that is directly originating from stellar outflows.

² http://www.cbata.harvard.edu/nova_list.html

³ <http://simbad.u-strasbg.fr/simbad/>

scale. Velocities are expressed in the local standard of rest frame (LSR).

The APEX spectra were reduced in the CLASS package within GILDAS⁴. The data reduction involved 0th order baseline subtraction and spectra averaging. Any faulty channels at spectral edges or caused by instrumental effects were blanked or interpolated between two nearest non-blanked channels. Sample APEX spectra are displayed in Figs. A.1–A.4 where we marked the corresponding 3σ noise levels.

APEX data for seventeen sources have been already reported in Kamiński et al. (2015). They are included here for completeness and consistency, and were re-processed using the procedures presented here.

2.2. IRAM observations and data reduction

Observations with the IRAM 30 m telescope and the EMIR dual-sideband receiver (Carter et al. 2012) were obtained in 6–11 August 2015. Fifty-eight objects observed with IRAM are listed in Table 2 and include 49 classical novae. Spectra for each linear polarization covered the same spectral range. The Fast Fourier Transform Spectrometer (FTS, Klein et al. 2012) and the WILMA correlator were used in parallel as backends. The FTS was used as the primary spectrometer, while WILMA data were used for reference since it covered a smaller part of the band (7.5 GHz) than FTS (16 GHz). WILMA spectra, as free from a platforming effect, were analyzed carefully, too. All IRAM observations were obtained using wobbler switching with OFF positions located azimuthally 110'' away from the central ON position.

The spectral setups used are listed in Table 3. All objects were observed with the setup whose lower side band was centered on the HCN(1–0) transition at 88.63160230 GHz; it serendipitously covered also the 1–0 transitions of H¹³CN and HNC (cf. Fig. A.5). For six objects, additional spectra were obtained in the ¹²CO(1–0) transition at 115.2712018 GHz; the corresponding lower sideband spectra covered also the ¹³CO(1–0) transition at 110.20135430 GHz.

All data reduction procedures were performed using CLASS and involved a low-order baseline subtraction and averaging. The FTS spectra required applying a deplatforming routine. While searching for broad nova lines, we used Hanning smoothing to reduce the resolution to about 30 km s⁻¹. Spectra of all objects observed in the ¹²CO(1–0) transition and a sample of spectra with the HCN(1–0) setup are displayed in Figs. A.5–A.8 together with marked 3σ noise levels calculated for the entire spectrum. Owing to the changing atmospheric transparency with wavelength, the noise levels change over the spectrum, especially in the CO(1–0) setup (cf. Fig. A.7).

2.3. Single-dish survey results: no detection of nova lines

To search for broad lines expected from classical novae outflows, we analyzed the spectra at a reduced spectral resolution of about 30 km s⁻¹. Except for CK Vul, known to have broad molecular emission from earlier studies, none of our survey targets shows broad features that can be associated with a nova system.

The measured rms noise levels for APEX spectra are listed in Table 4. The rms noise levels for the CO(3–2) spectra are relatively low, of 1–6 mK. The observations of CO(4–3) are much less constraining due to a lower atmosphere transparency at the respective frequencies. The IRAM observations in the CO(1–0)

line for a handful of objects are comparatively deep to the best APEX spectra, with global rms noise levels listed in Table 6. The noise levels are several times smaller near the rest frequency of the CO(1–0). The upper limits on HCN emission can be derived from the rms values listed in Table 5.

The southern part of the survey constitutes the largest sample of novae and related objects that were checked for the presence of rotational lines of CO. The noise levels achieved in our CO survey are one order of magnitude lower than in earlier observations of classical novae (e.g. Shore & Braine 1992). The IRAM survey of northern sources in the HCN(1–0) transition is the first one where lines other than those of CO were targeted for a large sample of classical novae.

Our upper limits on the molecular emission are not easily convertible to the limits on the total molecular mass because no direct information about the flow velocity, envelope size, and gas excitation temperature are known for individual objects. Here, we make an attempt to make such a conversion for a model nova representative of our survey. By referring to Gaia distances to nearly half of our sources in Schaefer (2018), we find that our typical classical nova is at a distance of 2 kpc. We further assume a typical flow velocity of $\Delta V = 1000$ km s⁻¹. Then, with an age of our typical nova remnant of about 50 yr, the shell has a size of 0.1 pc. In the optically thin limit, the mass of molecular material can be calculated as

$$M_{\text{mol}} = \frac{8\pi k \mu m_{\text{H}} Z(T_{\text{ex}}) \nu^2 \exp(E_u/T_{\text{ex}}) \eta_{\text{mb}} W a \left(\frac{\theta_{\text{beam}}}{\theta_{\text{source}}}\right)^2}{hc^3 g_u A_{ul}}$$

where

$$W = \int T_A^* dv \approx 3 \times \text{rms} \times 2 \times \Delta V$$

is the integrated intensity within the line profile, assuming a rectangular feature with a peak intensity equal to three times the measured noise level. k , h , and c are the Boltzmann and Planck constants, and the light speed, respectively; A_{ul} , g_u , E_u , and ν are Einstein coefficient, upper level statistical weight, energy (in K) of the upper level, and frequency of the considered transition; Z is the partition function at the excitation temperature T_{ex} ; the angular beam size is designated as θ_{beam} while the source angular size is θ_{source} ; μ is the molecular weight and m_{H} is the mass of hydrogen atom; a is the source projected area; both a and θ_{source} depend on the distance. We considered excitation temperatures of 10, 75, and 150 K to calculate rough upper limits on the total masses of CO from the CO(1–0) and (3–2) transitions and of HCN based on the HCN(1–0) spectra. The results are presented in Table 7.

The most constraining were the sensitive observations in CO(3–2), which indicate that the CO mass must be lower than $10^{-5} M_{\odot}$. For a CO fractional abundance relative to HI+H₂ of 10^{-4} (cf. Pontefract & Rawlings 2004), one obtains upper mass limits on molecular matter on the order of $0.1 M_{\odot}$. This value is not that constraining, given that a typical classical nova is thought to eject a total mass of $\lesssim 10^{-3} M_{\odot}$. However, the CO fractional abundance in a gas heavily enhanced in CNO burning product does not have to be close to that known from other circumstellar environments. The fractional abundance of HCN in classical novae is even more uncertain (cf. Schöier et al. 2013), but the upper limits we get are comparable or worse in constraining the molecular mass than the CO(3–2) data. Molecular gas in classical novae is not easily observable with current single-dish telescopes.

Our survey can also be compared to observations of the rovibrational band of CO at NIR wavelengths. As an example,

⁴ <https://www.iram.fr/IRAMFR/GILDAS>

we choose the case of V5668 Sgr whose prominent CO first-overtone emission was observed about a week after maximum light and was analyzed in Banerjee et al. (2016). The emission is thought to arise from a source of the size of 42 mas, in an outflow with an excitation temperature of about 4000 K and an expansion velocity $\Delta V=530 \text{ km s}^{-1}$. At the CO column density of $2 \times 10^{19} \text{ cm}^{-2}$ and assuming LTE conditions, the corresponding mm-wave emission in CO(1–0) observed by IRAM would have a peak antenna temperature of $0.5 \mu\text{K}$. Analogously, the CO(3–2) line emission observed with APEX would reach $43 \mu\text{K}$ (T_A^*). These extremely low values are a consequence of the high temperature and small source size, illustrating how ambitious it is to detect molecular emission from a nova shortly after the outburst. Let us however assume that the CO gas observed at NIR wavelengths survives for the next 50 years, decreases its gas temperature to 30 K, and expands into a source of a size of $2''75$. The size was calculated for free gas expansion at the distance of 2 kpc (cf. Banerjee et al. 2016). For such a source, the predicted peak antenna temperatures are of 0.1 and 0.3 K, well within the reach of our survey. Admittedly, V5668 Sgr is the most optimistic case with a particularly high molecular abundance and we have arbitrarily chosen the excitation temperature at which mm and submm lines are strong. Given the large number of observed novae, we would expect however to see a few objects with emission above our detection limits. That we did not detect any such source is possibly due to the decay of CO in later phases of ejecta expansion and much smaller filling factors (or a smaller source size) than we assumed. Indeed, chemical models of CO evolution of Pontefract & Rawlings (2004) predict high CO abundances only till ≈ 10 days after the eruption, after which they drop by at least two orders of magnitude. With some caution, results of our survey give qualitative support to such behavior.

2.4. Red-nova connection

The survey can be interpreted also in the context of red novae research. Nova 1670 or CK Vul had long been considered a classical nova until in 2014 strong mm-wave molecular emission was discovered in the object (Kamiński et al. 2015). This and other observational characteristics of the object led to the interpretation that instead of being a classical nova, CK Vul is a remnant of a stellar merger (Kamiński et al. 2018b, 2021) and its 1670–72 outburst can be classified as belonging to the group of (luminous) red novae (Kamiński et al. 2018a; Pastorello et al. 2019). Our survey can then be treated as a search for CK Vul analogs among historical novae, some of which could have been misidentified, especially if the nova event was not followed up spectroscopically sufficiently long. Since this experiment gave a negative result, objects similar to CK Vul must be very rare in the Galaxy. Indeed, luminous red novae outbursts are expected to occur only twice a decade (Howitt et al. 2020a). More systematic searches of red novae among historical objects classified as classical novae can improve our statistics of stellar mergers (cf. Kochanek et al. 2014; Howitt et al. 2020b).

Among the targets observed with APEX is V1148 Sgr, a nova from 1943 reported by Mayall (1949) and whose observations suggest that it could have been a red nova (Kimeswenger 2007). The exact position of the nova is uncertain. Although all the disputed positions of the remnant were well within the APEX beam, we do not detect any strong circumstellar emission in the CO transitions. This strongly advocates against a red nova classification of V1148 Sgr.

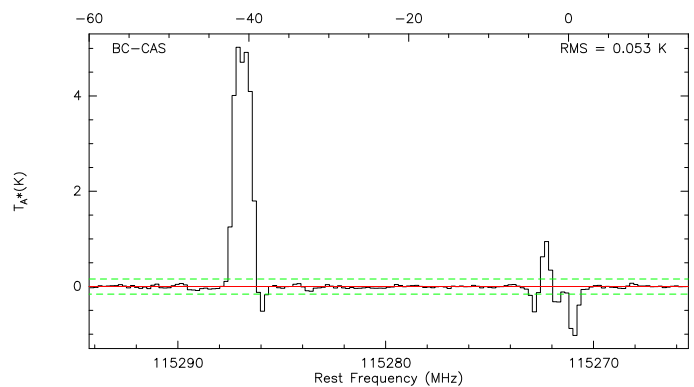


Fig. 1. The IRAM spectrum of BC Cas with ISM features of CO(1–0). The top axis gives LSR velocity with respect to the rest frequency of the CO transition. The dashed lines indicate the local 3σ noise level.

2.5. Observations of interstellar clouds

Data gathered for our entire sample of targets resulted in no detection of broad molecular emission that would be expected from classical novae shells. However, in the spectra of ten targets we observed narrow features which most likely arise in the foreground or background interstellar medium (ISM). This is not surprising as these objects are located close to the Galactic plane. The spectra are shown in Figs. 1–3. Some narrow spectral features appear in “absorption” when observed in one of the off-source wobbler positions. Below, we summarize the detected ISM features.

- In the direction of BC Cas, we detected $^{12}\text{CO}(1-0)$ features near -3 and -42 km s^{-1} (Fig. 1), the stronger of which is also detected in the isotopolog line of $^{13}\text{CO}(1-0)$ at $\approx -42 \text{ km s}^{-1}$ (Fig. A.8). The main line has the highest peak intensity among all observed ISM features in our survey and is optically thick based on the intensity ratio of the two observed CO isotopologs. This is in accord with BC Cas being a highly-reddened nova ($A_V=3.7$ mag) seen towards a star-forming region (Kato & Kojiguchi 2020).
- The spectra of CP Pup, RS Car, and AT Sgr show narrow emission and absorption features of CO(3–2) which combine into a P-Cyg type profiles (Fig. 2). This profile shape is a consequence of a small velocity difference between the ISM cloud velocity at the ON and OFF wobbler positions. The lines have a FWHM of $0.7-1.1 \text{ km s}^{-1}$, typical for the translucent ISM (cf. Snow & McCall 2006). Emission is observed at 8.8 km s^{-1} in CP Pup, at -11.8 km s^{-1} in RS Car, and at 12.0 km s^{-1} in AT Sgr. The lack of the corresponding CO(4–3) lines at our sensitivities (implying a line ratio of ≥ 2) is consistent with origin in a diffuse or translucent cloud.
- An absorption line centered at $\approx -38 \text{ km s}^{-1}$ and with a FWHM of 2 km s^{-1} is visible in the CO(3–2) spectrum of the recurrent nova IM Nor. A similar CO(3–2) feature is seen in the spectrum of V729 Sco at 19 km s^{-1} . The responsible ISM clouds are located in one of the wobbler OFF positions and do not necessarily cross the direction towards the novae.
- In the spectrum of a reddened nova V365 Car (Zwitter & Munari 1996), we found emission and absorption combining into an inverse P-Cyg profile. This again is a consequence of the ISM cloud extending between the ON and OFF wobbler positions with a small velocity gradient. Both emission and absorption components appear double, but the absorption component (OFF) is stronger. The emission component is centered near -25 km s^{-1} . No CO(4–3) emission is seen.

- The spectrum of V1148 Sgr shows two emission components, one centered at 21 km s^{-1} and with a FWHM of 3 km s^{-1} , and another narrow feature combining absorption and emission in $6\text{--}9 \text{ km s}^{-1}$. The emission lines are the weakest features detected in our survey.
- Two targets, AP Cru and V732 Sgr, show ISM features in both the CO(3–2) and CO(4–3) transitions (Fig. 3). While the line intensity ratio in AP Cru is not unusual for cool low-density ISM, the emission towards V732 Sgr is almost equal in both transitions, indicating a warmer interstellar environment. The case of V732 Sgr is discussed in more detail below.

2.5.1. Emission towards V732 Sgr

Spectra of V732 Sgr centered at the CO(3–2) and (4–3) transitions are shown in the two bottom panels of Fig. 3. Both spectra display a broad (FWHM $\approx 12 \text{ km s}^{-1}$) line centered near 62 km s^{-1} and several very narrow lines that appear as emission or absorption between 0 and 22 km s^{-1} . Additionally, the spectrum centered on the CO(3–2) transition shows a marginally significant feature near 111 km s^{-1} . Given the relatively broad profile of the CO lines near 62 km s^{-1} and a relatively high intensity of the CO(4–3) transition, this component is reminiscent of lines observed from envelopes of asymptotic-giant-branch (AGB) stars. However, CO emission towards V732 Sgr is known since the early 1990s, when it was mapped with SEST in the CO(1–0) transition, to be of interstellar origin (Weight et al. 1993; Albinson et al. 1994). The maps show that the molecular cloud is extended ($10' \times 3.5'$) and massive ($10^4 M_{\odot}$), and thus it cannot be directly associated with the nova. Interestingly, however, ≈ 100 days after V732 Sgr erupted in 1936, a weak light echo was visible for about 30 days (Swope 1940). The echoing medium was most likely associated with the giant interstellar cloud observed with SEST with APEX. The presence of light echo make V732 Sgr very similar to the nearby Nova Persei 1901 (GK Per), which we discuss in more detail in Sect. 3. All the novae for which ISM emission has been detected (including NQ Vul; Nielbock & Schmidtobreick 2003) are candidates to have been associated with a light echo (some could have been easily overlooked). Except GK Per and V732 Sgr, none of our sources with ISM detection was targeted for an echo search (van den Bergh 1977; Schaefer 1988). The light echo can arise only in clouds relatively close, up to tens of parsecs (Schaefer 1988).

Table 1. Objects observed with APEX.

Object	ID	CDS type	Observation date	RA (J2000)	Dec (J2000)
NOVA Cir 1914	AICIR	Nova	13-Jul-2016	14:49:31.2	-68:51:35.9
V* AP Cru	APCRU	Nova	09-Jun-2015	12:31:20.5	-64:26:25.2
V* AT Sgr	ATSGR	Nova	14-Jul-2016	18:03:30.8	-26:28:28.5
V* BD Pav	BDPAV	CataclyV*	10-Jun-2015	18:43:11.9	-57:30:44.9
V* CG CMa ^{a b}	CG-CMA	DwarfNova	24-Aug-2014	07:04:05.0	-23:45:34.6
NOVA Vel 1905 ^a	CN-VEL	Nova	24-Aug-2014, 09-Jun-2015	11:02:38.5	-54:23:09.5
V* CP Pup	CPPUP	Nova	08-Jun-2015	08:11:46.1	-35:21:04.9
NOVA Vel 1940 ^a	CQ-VEL	Nova	26-Aug-2014	08:58:50.9	-53:20:17.8
V* DY Pup ^a	DY-PUP	Nova	25-Aug-2014, 08-Jun-2015	08:13:48.5	-26:33:56.5
NOVA Sgr 1926	FMSGR	Nova	13-Jul-2016	18:17:18.1	-23:38:27.0
NOVA Mus 1983 ^a	GQ-MUS	Nova	28-Aug-2014	11:52:02.3	-67:12:20.2
V* GR Sgr	GRSGR	Nova	13-Jul-2016	18:22:58.5	-25:34:47.3
V* GU Mus ^{a b}	GU-MUS	HMXB	24-Aug-2014	11:26:26.6	-68:40:32.3
NOVA Sgr 1900	HSSGR	Nova	13-Jul-2016	18:28:03.4	-21:34:24.7
NOVA Nor 1893	ILNOR	Nova	07-Jul-2016	15:29:23.1	-50:35:00.7
NOVA Nor 1920	IMNOR	Nova	07-Jul-2016	15:39:26.4	-52:19:17.9
V* LZ Mus ^a	LZ-MUS	Nova	24-Aug-2014	11:56:09.2	-65:34:20.1
NOVA Cen 1931	MTCEN	Nova	30-Jun-2016	11:44:00.8	-60:33:39.5
V* RR Pic ^a	RR-PIC	Nova	25-Aug-2014	06:35:36.0	-62:38:24.3
V* RR Tel	RRTEL	Symbiotic*	10-Jun-2015	20:04:18.5	-55:43:33.2
NOVA Car 1895	RSCAR	Nova	30-Jun-2016	11:08:06.6	-61:56:04.6
NOVA Pyx 1890 ^a	T-PYX	Nova	24-Aug-2014	09:04:41.5	-32:22:47.5
V* TV Crv ^a	TV-CRV	DwarfNova	24-Aug-2014	12:20:24.1	-18:27:02.0
V* U Sco	USCO	CataclyV*	10-Jun-2015	16:22:30.8	-17:52:43.2
NOVA Sgr 1905	V1015SGR	Nova	06-Jul-2016	18:09:02.0	-32:28:32.0
NOVA Sgr 1899	V1016SGR	Nova	13-Jul-2016	18:19:57.6	-25:11:14.6
V* V1017 Sgr	V1017SGR	Nova	13-Jul-2016	18:32:04.4	-29:23:12.5
NOVA Cen 2007 ^a	V1065CEN	Nova	24-Aug-2014	11:43:10.3	-58:04:04.3
V* V1148 Sgr	V1148SGR	Nova	04-Apr-2015	18:09:05.8	-25:59:08.0
NOVA Sgr 1945 a	V1149SGR	Nova	13-Jul-2016	18:18:30.4	-28:17:17.0
V* V1151 Sgr	V1151SGR	Nova	14-Jul-2016	18:25:23.7	-20:11:59.3
NOVA Sgr 1928	V1583SGR	Nova	14-Jul-2016	18:15:26.3	-23:23:18.0
V* V351 Car ^a	V351-CAR	Mira	28-Aug-2014	10:45:19.1	-72:03:56.0
V* V359 Cen ^a	V359-CEN	DwarfNova	24-Aug-2014	11:58:15.3	-41:46:08.4
NOVA Sgr 1927	V363SGR	Nova	11-Jun-2015, 01-Jul-2016	19:11:16.3	-29:50:00.0
V* V365 Car	V365CAR	Nova	09-Jun-2015, 30-Jun-2016	11:03:16.7	-58:27:24.9
NOVA Sco 1901 ^a	V382SCO	Nova	13-Jul-2016	17:51:56.1	-35:25:05.4
NOVA Vel 1999	V382-VEL	Nova	28-Aug-2014, 08-Sep-2014	10:44:48.3	-52:25:30.7
NOVA Sgr 1893	V384SCO	Nova	14-Jul-2016	18:01:43.1	-35:39:27.8
V* V522 Sgr	V522SGR	Nova	11-Jun-2015, 01-Jul-2016	18:48:00.4	-25:22:21.9
NOVA Oph 1940	V553OPH	Nova	01-Jul-2016	17:42:53.5	-24:51:26.2
NOVA Pup 2007 b ^a	V598-PUP	Nova	25-Aug-2014	07:05:42.5	-38:14:39.4
NOVA Sco 1944	V696SCO	Nova	13-Jul-2016	17:53:11.5	-35:50:14.4
NOVA Sco 1941	V697SCO	Nova	13-Jul-2016	17:51:21.8	-37:24:55.2
NOVA Sco 1922	V707SCO	Nova	06-Jul-2016	17:48:26.3	-36:37:54.9
NOVA Sco 1906	V711SCO	Nova	14-Jul-2016	17:54:06.1	-34:21:15.5
V* V729 Sco	V729SCO	V*	10-Jun-2015, 01-Jul-2016	17:22:02.6	-32:05:48.8
NOVA Sgr 1936	V732SGR	Nova	13-Jul-2016	17:56:07.5	-27:22:16.1
V* V733 Sco	V733SCO	CandidateMi*	06-Jul-2016	17:39:42.8	-35:52:38.4
NOVA Sgr 1933	V737SGR	Nova	14-Jul-2016	18:07:08.6	-28:44:52.3
V* V745 Sco	V745SCO	LPV*	13-Jul-2016	17:55:22.2	-33:14:58.5
NOVA Sgr 1937	V787SGR	Nova	14-Jul-2016	18:00:02.2	-30:30:31.0
V* V794 Oph	V794OPH	Nova	01-Jul-2016	17:38:49.2	-22:50:48.9
V* V840 Oph	V840OPH	Nova	10-Jun-2015	16:54:43.9	-29:37:26.8
NOVA Sgr 1941	V909SGR	Nova	13-Jul-2016	18:25:52.3	-35:01:27.0
V* V941 Sgr	V941SGR	Mira	13-Jul-2016	18:34:43.4	-29:34:49.1
NOVA Sgr 1910	V999SGR	Nova	13-Jul-2016	18:00:05.5	-27:33:14.0
V* VX For ^a	VX-FOR	DwarfNova	24-Aug-2014	03:26:45.7	-34:26:25.2
V* WX Cet ^a	WX-CET	DwarfNova	24-Aug-2014	01:17:04.1	-17:56:23.0

Notes. Objects were observed in the CO(3–2), CO(3–2) OSB, CO(4–3), CO(4–3) OSB setups. ^(a) Observation reported in Kamiński et al. (2015).

^(b) Observed only in CO(3–2), CO(3–2) OSB setups.

Table 2. Objects observed with IRAM.

Object	ID	CDS type	Observation date	RA (J2000)	Dec (J2000)	Target lines
V* BC Cas	BC-CAS	Nova	10-Aug-2015	23:51:17.4	60:18:10.0	HCN(1 – 0), ¹² CO(1 – 0)
NOVA Aql 1917	CI-AQL	Nova	09-Aug-2015	18:52:03.5	01:28:39.4	HCN(1 – 0)
V* CI Gem	CI-GEM	DwarfNova	10-Aug-2015	06:30:05.8	22:18:50.7	HCN(1 – 0)
V* CK Vul	CK-VUL	CataclyV*	07-Aug-2015	19:47:37.9	27:18:48.0	HCN(1 – 0)
V* CP Lac	CP-LAC	Nova	09-Aug-2015	22:15:41.0	55:37:01.3	HCN(1 – 0), ¹² CO(1 – 0)
V* DI Lac	DI-LAC	Nova	10-Aug-2015	22:35:48.4	52:42:59.6	HCN(1 – 0), ¹² CO(1 – 0)
NOVA Gem 1903	DM-GEM	Nova	10-Aug-2015	06:44:12.0	29:56:41.8	HCN(1 – 0)
V* DN Gem	DN-GEM	Nova	10-Aug-2015	06:54:54.3	32:08:27.9	HCN(1 – 0)
NOVA Ser 1960	DZ-SER	Nova	07-Aug-2015	18:00:58.8	10:33:52.1	HCN(1 – 0)
V* EL Aql	EL-AQL	Nova	09-Aug-2015	18:56:02.0	03:19:20.5	HCN(1 – 0)
V* GK Per	GK-PER	Nova	07-Aug-2015	03:31:12.0	43:54:15.4	HCN(1 – 0)
NOVA Ori 1916	GR-ORI	Nova	11-Aug-2015	05:21:35.2	01:10:08.6	HCN(1 – 0)
NOVA Sge 1977	HS-SGE	Nova	10-Aug-2015	19:39:22.0	18:07:53.9	HCN(1 – 0)
NOVA Mon 1942	KT-MON	Nova	11-Aug-2015	06:25:18.4	05:26:31.7	HCN(1 – 0)
NOVA And 1986	OS-AND	Nova	11-Aug-2015	03:12:05.7	47:28:19.7	HCN(1 – 0)
V* PQ And	PQ-AND	DwarfNova	07-Aug-2015	02:29:29.6	40:02:40.9	HCN(1 – 0)
V* Q Cyg	Q-CYG	Nova	09-Aug-2015	21:41:43.9	42:50:29.0	HCN(1 – 0)
V* RS Oph	RS-OPH	Nova	07-Aug-2015	17:50:13.1	06:42:28.4	HCN(1 – 0)
NOVA UMi 1956	RW-UMI	Nova	10-Aug-2015	16:47:54.7	77:02:12.1	HCN(1 – 0)
NOVA Sge 1916	SS-SGE	Nova	10-Aug-2015	19:39:08.3	16:42:40.5	HCN(1 – 0)
NOVA Gem 1857	SY-GEM	Nova	10-Aug-2015	06:40:39.1	31:10:55.3	HCN(1 – 0)
NOVA Per 1853	SZ-PER	Nova	07-Aug-2015	03:47:06.3	34:19:17.9	HCN(1 – 0)
V* UW Per	UW-PER	DwarfNova	07-Aug-2015	02:12:29.5	57:05:19.7	HCN(1 – 0)
V* UZ Tri	UZ-TRI	Nova	10-Aug-2015	01:58:24.6	33:31:30.0	HCN(1 – 0)
V* V1059 Sgr	V1059-SGR	Nova	09-Aug-2015	19:01:50.5	13:09:41.9	HCN(1 – 0)
V* V1229 Aql	V1229-AQL	Nova	09-Aug-2015	19:24:44.5	04:14:48.6	HCN(1 – 0)
V* V1378 Aql	V1378-AQL	Nova	09-Aug-2015	19:16:35.4	03:43:26.3	HCN(1 – 0)
V* V1449 Cyg	V1449-CYG	DwarfNova	09-Aug-2015	19:49:16.5	34:10:49.1	HCN(1 – 0)
V* V1500 Cyg	V1500-CYG	Nova	09-Aug-2015	21:11:36.3	48:09:05.8	HCN(1 – 0)
NOVA Cyg 1978	V1668-CYG	Nova	09-Aug-2015	21:42:35.2	44:01:54.9	HCN(1 – 0)
V* V1697 Cyg	V1697-CYG	DwarfNova	09-Aug-2015	20:43:16.9	42:42:38.9	HCN(1 – 0)
V* V1974 Cyg	V1974-CYG	Nova	09-Aug-2015	20:30:31.6	52:37:51.3	HCN(1 – 0)
NOVA Oph 1994	V2313-OPH	Nova	08-Aug-2015	17:35:44.6	19:19:34.0	HCN(1 – 0)
NOVA Cyg 2005	V2361-CYG	Nova	09-Aug-2015	20:09:19.0	39:48:52.9	HCN(1 – 0)
NOVA Cyg 2006	V2362-CYG	Nova	09-Aug-2015	21:11:32.3	44:48:03.6	HCN(1 – 0)
V* V2467 Cyg	V2467-CYG	Nova	09-Aug-2015	20:28:12.4	41:48:36.5	HCN(1 – 0)
PN K 3-25	V352-AQL	Symbiotic*	09-Aug-2015	19:13:33.6	02:18:12.9	HCN(1 – 0)
NOVA Her 1892	V360-HER	Nova	08-Aug-2015	17:16:38.0	24:26:47.2	HCN(1 – 0)
V* V368 Aql	V368-AQL	Nova	10-Aug-2015	19:26:34.4	07:36:13.8	HCN(1 – 0)
NOVA Per 1974	V400-PER	Nova	07-Aug-2015	03:07:38.1	47:07:38.8	HCN(1 – 0)
V* V446 Her	V446-HER	Nova	08-Aug-2015	18:57:21.5	13:14:29.8	HCN(1 – 0)
NOVA Cyg 1948	V465-CYG	Nova	09-Aug-2015	19:52:37.6	36:33:52.6	HCN(1 – 0)
V* V476 Cyg	V476-CYG	Nova	09-Aug-2015	19:58:24.4	53:37:07.4	HCN(1 – 0)
NOVA Aql 1943	V500-AQL	Nova	10-Aug-2015	19:52:27.8	08:28:46.3	HCN(1 – 0)
NOVA Ori 1667	V529-ORI	Nova	10-Aug-2015	05:58:20.1	20:15:45.4	HCN(1 – 0)
HD 176779	V604-AQL	Nova	09-Aug-2015	19:02:06.3	04:26:43.2	HCN(1 – 0)
HD 181419	V606-AQL	Nova	09-Aug-2015	19:20:24.2	00:08:07.0	HCN(1 – 0)
V* V630 Cas	V630-CAS	DwarfNova	10-Aug-2015	23:48:51.9	51:27:39.1	HCN(1 – 0), ¹² CO(1 – 0)
V* V705 Cas	V705-CAS	Nova	11-Aug-2015	23:41:47.1	57:30:59.5	HCN(1 – 0)
V* V723 Cas	V723-CAS	Nova	10-Aug-2015	01:05:05.3	54:00:40.2	HCN(1 – 0), ¹² CO(1 – 0)
NOVA Her 1991	V838-HER	Nova	08-Aug-2015	18:46:31.5	12:14:00.6	HCN(1 – 0)
NOVA Aql 1951	V841-AQL	Nova	09-Aug-2015	19:07:39.7	10:29:43.7	HCN(1 – 0)
NOVA Oph 1919	V849-OPH	Nova	08-Aug-2015	18:14:07.1	11:36:42.7	HCN(1 – 0)
NOVA Per 1887	V-PER	Nova	10-Aug-2015	02:01:53.7	56:44:04.0	HCN(1 – 0), ¹² CO(1 – 0)
V* VY Aqr	VY-AQR	DwarfNova	06-Aug-2015	21:12:09.2	08:49:36.7	HCN(1 – 0)
NOVA Gem 1856	VZ-GEM	Nova	11-Aug-2015	08:07:47.0	30:50:54.0	HCN(1 – 0)
NOVA Ari 1855	W-ARI	Nova	07-Aug-2015	03:20:45.1	28:57:13.9	HCN(1 – 0)
NOVA Sge 1783	WY-SGE	Nova	10-Aug-2015	19:32:43.8	17:44:55.8	HCN(1 – 0)

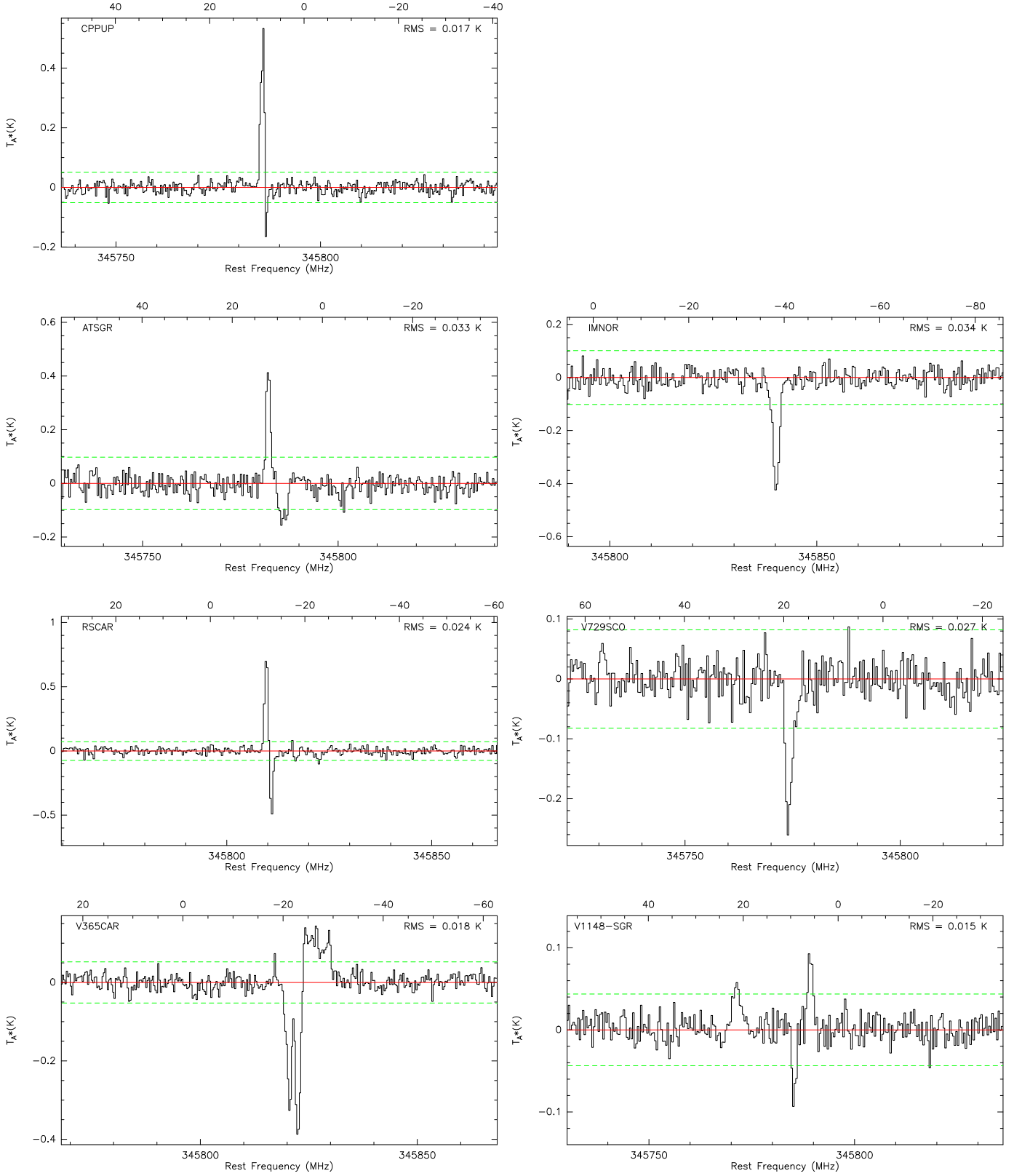


Fig. 2. APEX spectra with ISM features of CO(3–2). The top axes give LSR velocity with respect to the rest frequency of the corresponding CO transition. Dashed lines indicate local 3σ noise levels. The rms values are provided for the baseline outside the ISM features and for the current binning.

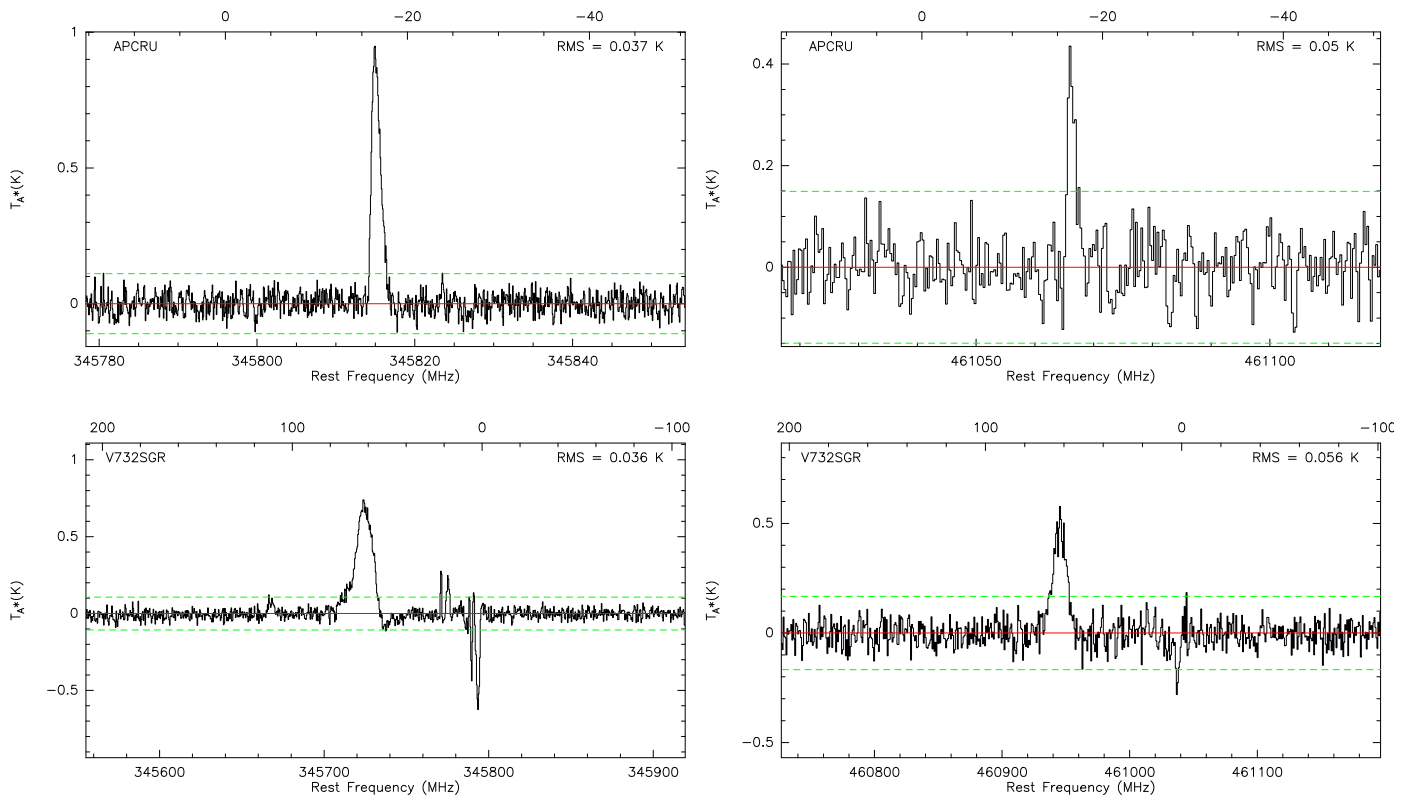


Fig. 3. Spectra with ISM features detected on CO(3–2) (left) and CO(4–3) (right) in AP Cru (top) and V732 Sgr (bottom). The top axes give LSR velocity with respect to the rest frequency of the corresponding CO transition. Dashed lines indicate local 3σ noise levels.

Table 3. Spectral setups used in the survey.

Telescope	Setup name	Range (GHz)	Beam (")	η_{mb}
APEX	CO(3–2) OSB	331.8–335.8	18.7	0.70
APEX	CO(3–2)	343.8–348.8	18.0	0.69
APEX	CO(4–3)	459.0–463.0	13.5	0.64
APEX	CO(4–3) OSB	471.0–475.0	13.2	0.63
IRAM	HCN(1–0)	83.1–91.0	27.8	0.85
IRAM	HCN(1–0) USB	98.8–106.6	24.3	0.84
IRAM	CO(1–0) LSB	94.1–101.9	25.5	0.84
IRAM	CO(1–0) USB	109.8–117.5	21.3	0.83

Table 4. Noise levels in APEX observations.

Object	rms (mK)			
	CO32	CO32 OSB	CO43	CO43 OSB
NOVA Cir 1914	6.49	7.52	23.19	120.60
V* AT Sgr	3.55	4.17	9.48	33.44
V* CG CMa	1.57	1.87		
NOVA Vel 1905	1.28	2.17	2.45	9.73
NOVA Vel 1940	1.67	1.83	4.34	15.45
V* DY Pup	1.90	1.36	2.58	9.1
NOVA Sgr 1926	3.87	4.08	8.79	35.42
NOVA Mus 1983	2.40	3.04	6.46	19.67
V* GR Sgr	2.56	3.29	8.87	35.24
V* GU Mus	2.11	2.53		
NOVA Sgr 1900	3.69	4.17	10.23	47.94
NOVA Nor 1893	3.86	3.92	10.74	65.30
NOVA Nor 1920	4.10	4.61	9.95	48.29
V* LZ Mus	2.45	2.82	10.86	43.82
NOVA Cen 1931	2.77	2.63	8.05	39.86
V* RR Pic	2.07	1.80	4.78	15.63
NOVA Car 1895	2.92	3.14	7.73	35.71
NOVA Pyx 1890	1.77	1.75	4.21	17.27
V* TV Crv	1.70	1.83	5.19	15.04
NOVA Sgr 1905	2.79	3.13	9.86	48.87
NOVA Sgr 1899	4.11	3.92	8.41	42.64
V* V1017 Sgr	2.43	2.91	6.09	22.74
NOVA Cen 2007	3.08	3.57	17.36	67.42
V* V1148 Sgr	1.75	1.58	2.97	9.31
NOVA Sgr 1945 a	3.33	3.40	5.36	16.59
V* V1151 Sgr	4.46	4.57	13.99	71.71
NOVA Sgr 1928	4.21	4.29	11.36	65.54
V* V351 Car	2.60	2.36	8.26	36.29
V* V359 Cen	1.68	1.85	4.35	13.84
NOVA Sgr 1927	3.07	3.63	17.23	107.46
V* V365 Car	2.88	2.01	3.6	12.62
NOVA Sco 1901	2.86	3.05	5.73	17.21
NOVA Vel 1999	1.06	2.03	4.06	33.58
NOVA Sgr 1893	3.94	4.82	13.10	64.73
V* V522 Sgr	4.62	5.05	28.57	120.05
NOVA Oph 1940	5.81	6.83	30.70	197.26
NOVA Pup 2007 b	1.59	1.85	3.73	10.60
NOVA Sco 1944	3.27	3.34	6.98	26.70
NOVA Sco 1941	3.33	3.09	5.57	23.98
NOVA Sco 1922	4.03	3.99	13.37	82.88
NOVA Sco 1906	4.12	4.32	11.00	58.49
V* V729 Sco	2.58	3.75	6	17.57
NOVA Sgr 1936	3.13	3.42	17.30	32.48
V* V733 Sco	4.05	4.94	12.78	69.67
NOVA Sgr 1933	4.26	3.69	9.47	36.23
V* V745 Sco	2.71	3.08	6.76	15.60
NOVA Sgr 1937	3.96	3.61	10.33	43.59
V* V794 Oph	5.07	7.11	27.27	184.94
NOVA Sgr 1941	3.17	3.59	8.13	30.68
V* V941 Sgr	3.90	4.12	11.39	55.70
NOVA Sgr 1910	3.55	3.75	7.11	34.40
V* VX For	2.05	2.34	5.87	24.96
V* WX Cet	1.84	1.68	4.91	12.56
V* CP Pup	1.98	2.02	3.33	12.91
V* AP Cru	2.90	2.80	6.18	19.73
V* U Sco	3.13	4.25	7.34	25.34
V* V840 Oph	3.65	3.72	7.39	30.64
V* BD Pav	4.19	5.25	14.33	83.76
V* RR Tel	4.52	4.57	10.02	62.0

Notes. Root-mean-square values are given per velocity bins of 30 km s^{-1} for CO(3–2) and CO(4–3), 31 km s^{-1} for CO(3–2) OSB, and 29 km s^{-1} for CO(4–3) OSB.

Table 5. Noise levels in IRAM spectra near the HCN(1–0) line.

Object	rms (mK)			
	WILMA		FTS	
	LSB	USB	LSB	USB
V* BC Cas	4.26	5.25	4.44	5.47
NOVA Aql 1917	3.83	4.51	3.98	4.80
V* CI Gem	4.76	5.74	4.87	6.04
V* CK Vul	7.10	8.33	7.51	9.43
V* CP Lac	3.29	4.03	3.37	4.14
V* DI Lac	4.08	4.64	3.24	3.73
NOVA Gem 1903	3.93	5.05	4.42	5.24
V* DN Gem	3.87	4.81	4.07	4.76
NOVA Ser 1960	7.29	8.44	7.65	9.48
V* EL Aql	3.90	4.11	4.03	4.72
V* GK Per	2.61	2.80	2.67	3.00
NOVA Ori 1916	6.24	7.75	7.02	7.69
NOVA Sge 1977	4.74	5.72	5.19	6.11
NOVA Mon 1942	5.54	6.63	6.04	7.01
NOVA And 1986	3.38	4.06	3.51	4.01
V* PQ And	2.40	2.85	2.64	2.99
V* Q Cyg	3.24	3.60	3.60	4.00
V* RS Oph	6.71	8.48	7.09	8.94
NOVA UMi 1956	5.21	6.11	5.41	6.45
NOVA Sge 1916	4.56	5.84	5.07	6.08
NOVA Gem 1857	4.15	5.30	4.44	5.35
NOVA Per 1853	2.58	2.79	2.61	3.08
V* UW Per	3.14	3.62	3.38	3.81
V* UZ Tri	5.59	6.57	6.02	6.97
V* V1059 Sgr	3.50	3.83	3.63	4.09
V* V1229 Aql	4.01	4.71	4.29	5.08
V* V1378 Aql	3.97	4.48	4.25	5.05
V* V1449 Cyg	3.30	4.17	3.69	4.19
V* V1500 Cyg	3.20	3.70	3.68	3.96
NOVA Cyg 1978	3.30	3.94	3.43	3.95
V* V1697 Cyg	3.39	3.77	3.71	4.31
V* V1974 Cyg	3.41	4.03	3.75	4.22
NOVA Oph 1994	7.53	9.25	7.50	9.56
NOVA Cyg 2005	3.36	3.94	3.51	4.18
NOVA Cyg 2006	3.11	4.23	3.51	4.13
V* V2467 Cyg	3.23	3.89	3.65	4.18
PN K 3-25	2.78	3.45	2.75	3.55
NOVA Her 1892	9.47	11.77	9.27	12.39
V* V368 Aql	4.57	5.67	4.71	6.03
NOVA Per 1974	3.20	3.73	3.40	3.91
V* V446 Her	3.46	4.11	3.61	4.16
NOVA Cyg 1948	2.36	2.87	2.60	3.02
V* V476 Cyg	3.43	4.10	3.63	4.64
NOVA Aql 1943	4.54	5.89	4.74	5.76
NOVA Ori 1667	4.17	5.47	4.83	5.96
HD 176779	3.69	4.39	3.96	4.83
HD 181419	4.03	4.41	4.14	4.90
V* V630 Cas	4.37	4.59	4.32	5.06
V* V705 Cas	3.31	4.10	3.49	4.11
V* V723 Cas	3.75	4.75	4.33	4.91
NOVA Her 1991	3.53	4.11	3.84	4.17
NOVA Aql 1951	3.62	3.79	3.85	4.31
NOVA Oph 1919	17.22	20.94	16.91	22.81
NOVA Per 1887	4.13	4.87	4.47	5.45
V* VY Aqr	2.65	3.18	2.98	3.46
NOVA Gem 1856	3.63	4.19	3.83	4.71
NOVA Ari 1855	2.69	2.92	2.77	3.28
NOVA Sge 1783	4.73	5.67	4.98	5.97

Notes. The noise rms values per 30 km s^{-1} are given for both backends used (they differ in coverage and baseline quality). The LSB values correspond to the spectra which covered the HCN(1–0) transition.

Table 6. Noise levels in IRAM spectra near the CO(1–0) line.

Object	rms (mK)				
	WILMA		FTS		CO10 ^a
	LSB	USB	LSB	USB	
V* BC Cas	2.21	3.14	2.38	16.06	6.22
V* CP Lac	2.29	3.47	2.22	10.39	6.87
V* DI Lac	2.13	3.12	2.27	11.10	7.56
V* V630 Cas	1.62	2.28	1.57	6.23	4.71
V* V723 Cas	2.13	2.88	2.16	8.81	6.68
NOVA Per 1887	2.11	2.96	2.52	10.15	7.09

Notes. The T_A^* noise rms values per 30 km s^{-1} are given for both backends used (they differ in coverage and baseline quality). The USB values correspond to the entire spectra which covered the CO(1–0) transition.^(a) The rms value measured in 114.27–116.27 GHz, near the rest frequency of the CO(1–0) transition and ignoring the ISM features.

Table 7. Upper limits on molecular mass in a model classical nova.

Observed transition	$3 \times \text{rms}$ (T_A^* , mK)	T_{ex} (K)	Mass limit (M_{\odot})
CO(3–2)	6	10	$M_{\text{CO}} < 9.0 \times 10^{-5}$
		75	$M_{\text{CO}} < 3.7 \times 10^{-5}$
		100	$M_{\text{CO}} < 5.8 \times 10^{-5}$
CO(1–0)	18	10	$M_{\text{CO}} < 3.0 \times 10^{-4}$
		75	$M_{\text{CO}} < 1.4 \times 10^{-3}$
		100	$M_{\text{CO}} < 2.6 \times 10^{-3}$
HCN(1–0)	9	10	$M_{\text{HCN}} < 1.0 \times 10^{-6}$
		75	$M_{\text{HCN}} < 5.3 \times 10^{-6}$
		100	$M_{\text{HCN}} < 1.0 \times 10^{-5}$

Notes. The $3 \times \text{rms}$ values are based on Tables 4–6.

3. CO maps around GK Per

3.1. Motivation

GK Per is a unique cataclysmic variable whose distance of 442 pc (Schaefer 2018) makes it the second-closest nova. The central binary consists of a magnetic white dwarf of $0.9\text{--}1.0 M_{\odot}$ (Wada et al. 2018; Álvarez-Hernández et al. 2021) and a K1 IV subgiant (Álvarez-Hernández et al. 2021). It erupted as a classical nova in 1901 and, as mentioned, is one of two known classical novae to have been associated with light echoes. The echoes reached a size of tens of arcseconds (Ritchey 1902). Since the middle of the last century, GK Per has experienced dwarf-nova outbursts every 1–3 yr (Šimon 2002). Nova ejecta was first observed in 1916 and remains visible to this day (Liimets et al. 2012; Shara et al. 2012). The Firework Nebula, as it is often referred to, has a size of nearly $100''$ and is considered the longest-lived remnant of a classical nova event. The highest gas velocities found in the remnant are of 2800 km s^{-1} but typical values are of about 1100 km s^{-1} .

GK Per is the only classical nova that has been claimed to have molecular gas in its immediate proximity long after its outburst⁵. The nature of its observed CO emission has been somewhat controversial. Observations of the CO $J = 2 - 1$ rotational line with the James Clerk Maxwell Telescope (JCMT) acquired in 1993 by Scott et al. (1994) revealed elongated symmetrical structures with two main “concentrations” connected by a bridge of emission $\approx 1'$ north of the object. The concentrations are located $3'$ east and west off GK Per. However, the emission region was not fully mapped; in particular, the concentrations are seen near the edges of the undersampled map, which puts into question the extent of the emission. Observed lines are narrow, with a FWHM of a few km s^{-1} , atypical for circumstellar envelopes. No large velocity gradients within the cloud were found. The molecular gas was proposed to be associated with a filamentary and dusty bipolar cloud of a size of $17'$ from which dust emission was first observed with the Infrared Astronomical Satellite (IRAS). This filamentary cloud was interpreted by Bode et al. (1987), Seaquist et al. (1989), and Dougherty et al. (1996) as a bipolar outflow or a planetary nebula (PN) from the nova system. Their argument was based mainly on the symmetry of the cloud’s morphology relative to GK Per. An atomic component of the cloud was also mapped in the 21 cm line of neutral hydrogen (H I) by Seaquist et al. (1989). In order to explain the very large extent and the very high mass of $3.8 M_{\odot}$ derived for the cloud, both highly atypical for classical novae, Dougherty et al. invoked a rather elaborate scenario where mass loss involving the secondary had occurred prior to the Nova 1901 event. They considered the binary to be then in the second Roche-lobe overflow phase, in which the mass transfer from the secondary, then of a mass of $1.3\text{--}1.5 M_{\odot}$, was sufficient to convert the white dwarf into a “born again” AGB star. Knowing the composition of the nebula would be of great value in order to verify this hypothesis. If the CO emission observed with the JCMT indeed represents such circumstellar gas, it could provide means to measure relevant isotopic ratios.

On the other hand, the CO emission near GK Per may be purely interstellar. In 1985 Hessman (1989) mapped in the CO(1–0) line the large-scale structure that was identified in IRAS maps. With the 4.9-m telescope of the Millimeter Wave Observatory, he mapped a much larger area than was covered

with JCMT, roughly of $40' \times 50'$ and at a resolution of $2''.6$. He only found a weak correspondence between the CO emission and the IRAS emission, which would be atypical for any circumstellar material. Hessman concluded that most of the CO material belonged to an interstellar cirrus cloud that is unrelated to the nova. This interpretation is not favored in the recent literature on GK Per.

Most recently, the vicinity of GK Per was mapped with the Wide-field Infrared Survey Explorer (WISE Wright et al. 2010) at a higher sensitivity and with better angular resolutions than with IRAS. WISE maps in $W3$ and $W4$ bands, at 12 and $22 \mu\text{m}$, respectively, readily show the same extended dusty cloud that was identified in IRAS data (Fig. 4). It has the appearance of an interstellar cirrus. However, at shorter wavelengths, that is at $3.4 \mu\text{m}$ ($W1$) and $4.6 \mu\text{m}$ ($W2$), WISE maps display a smaller bubble-like, bipolar structure centered on GK Per. Although weak in both bands, it is most readily present in the $W2$ image. The longer axis of the nebula is of about $15'$ and is oriented at a position angle of $\approx -30^{\circ}$. The structure appears irregular, with the southeastern lobe being bigger and of a width of about $7'$. The same bipolar structure was observed earlier in the $H\alpha$ filter (covering the $H\alpha$ line and the $[\text{N II}]$ doublet) and in the $[\text{O III}] \lambda 5007$ line by Tweedy (1995)⁶ and Bode et al. (2004). The observations imply that the optical emission is dominated by line emission of recombining low-density gas. Since the $W1$ and $W2$ bands also cover several emission lines, we cannot dismiss the possibility that the bipolar WISE structure is seen through IR emission lines. However, the southern part of the bipolar structure was seen in the light echoes in 1901–1902 and thus must contain dust grains. We assume that the mid-IR emission of this structure arises as continuum emission of relatively warm dust, warmer than the larger ISM cirrus seen in $W3$ and $W4$. Tweedy excluded the possibility that the observed feature represents a genuine PN, but later authors (e.g., Bode et al. 2004; Harvey et al. 2016; Dougherty et al. 1996; Álvarez-Hernández et al. 2021) challenged this conclusion. This nebula is smaller and much less massive than the dusty cloud seen in the IRAS images, but both structures have often been confused in the literature and named a planetary nebula interchangeably. Hereafter, we refer to the smaller structure as a planetary or bipolar nebula, and we call the larger-scale emission a cirrus.

Based solely on the morphology of the smaller nebula, there is little doubt that it is a signature of mass-loss activity in GK Per before the Nova 1901 event. The longer axis of the structure aligns well with the larger interstellar cirrus, perhaps causing the confusion in the literature. The molecular gas mapped earlier with the JCMT and reported in Scott et al. (1994), would be filling the bipolar lobes of the planetary nebula, with the concentration located closely to the main axis of the bipolar structure. This strongly suggests circumstellar origin of the CO gas, against the interpretation of Hessman (1989). With the presence of a PN now firmly established with the WISE maps, we decided to revisit the claim of the presence of circumstellar molecular gas around GK Per by obtaining new deeper maps of CO emission near GK Per.

3.2. Mapping observations

Mapping observations around GK Per were executed in 9, 10, 12 April 2021 and on 28 May 2021 with the IRAM 30 m telescope. The data were acquired within the IRAM program 155-20 (PI:

⁵ Evans (1997) claimed the presence of H_2 emission in DQ Her some 56 years after its eruption and based on imaging observations. The emission identification has never been confirmed spectroscopically, though.

⁶ Their Fig. 1 has an incorrectly assigned orientation. The maps have east up and north right.

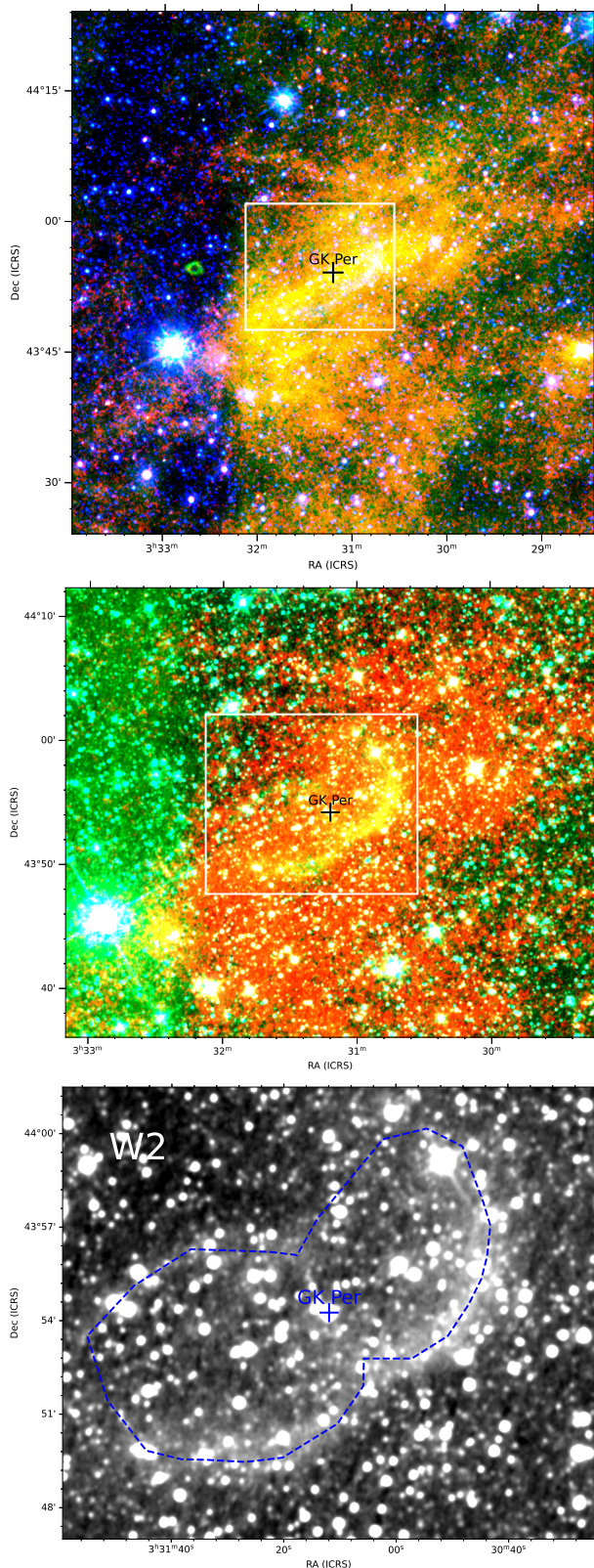


Fig. 4. WISE images of the field around GK Per. Top: A wide-angle view ($1^\circ \times 1^\circ$) with blue, green, and red colors representing signal in W2, W3, and W4 filters, respectively. It shows the large cirrus IS cloud reported earlier in IRAS observations. Middle: Closeup view with blue, green, and red showing W1, W2, and W4 images, respectively. In yellow, a bipolar structure is seen near the position of GK Per. Bottom: W2 image of the bipolar structure. Its shape was arbitrarily outlined with a dashed line. The northern edge is not well-defined. The field shown ($17:0 \times 14:5$) corresponds to the white boxes drawn in two upper panels. All panels show intensity in linear scale.

H. Mazurek). We used the EMIR E90 and E230 receivers simultaneously and centered them near the CO $J = 1 - 0$ and $2 - 1$, transitions, which have rest frequencies of 115.2712 and 230.5380 GHz, respectively. The FTS and WILMA backends were used as spectrometers with the FTS having a native resolution of 0.5 and 0.25 km s^{-1} for the CO(1–0) and (2–1) spectra, respectively. Although effectively the spectral ranges of 113.522–117.570 GHz and 228.240–236.016 GHz were covered, no lines other than the targeted ^{12}CO transitions were detected. Regular pointing observations were obtained at the beginning and during mapping runs. Focus calibration on a planet was secured before each observing session.

The maps were obtained in the on-the-fly (OTF) mode, with a reference OFF position at (RA, Dec) offsets of ($700''$, $350''$) from the position of GK Per. The reference position was checked earlier to be free of any molecular emission. An area within a field of view of $1128''.8 \times 987''.0$ was mapped in two smaller parts, each with multiple coverages obtained in orthogonal directions of the beam scanning. Relative to the position of GK Per, the map is composed of two rectangular regions at (RA, Dec) offsets of ($610''$ to $10''$, $-410''$ to $210''$) and ($80''$ to $-450''$, $-150''$ to $500''$) and with some overlap between the two areas near the position of the nova. The map sampling was set to $8''.5$, which is optimal for the beam size of the CO(1–0) observations ($21''.3$). Owing to several coverages of each part of the map at a slightly different offset (of a few arcsec), the grid of observed positions is effectively denser, allowing also to obtain a map of CO(2–1) that, with the beam size of $10''.7$, is only slightly undersampled. The data were calibrated every 8 min and registered in T_A^* units. The conversion of the CO(2–1) data to the main beam temperature units requires $\eta_{\text{mb}} = 0.64$ (cf. Table 3). All data were reduced in CLASS, including baseline subtraction, spectra averaging and rebinning, and map gridding. The final rms noise in the CO(1–0) cube is of 0.22 K (T_A^*) at 0.45 km s^{-1} binning; for the CO(2–1) cube, it is 0.41 K per 0.45 km s^{-1} .

3.3. Results of CO mapping

At the position of GK Per, no broad emission lines are found that could originate in the nova system. A narrow and weak CO(1–0) line is seen at this position and originates in the interstellar cloud.

Both maps show interstellar clouds emission over most of the mapped area and in the $1.5\text{--}8.0 \text{ km s}^{-1}$ range. Here we focus on the better sampled CO(1–0) map, as the CO(2–1) map looks qualitatively the same. The total intensity CO(1–0) map is shown in Fig. 5. It displays a ridge of molecular emission spreading over most of the mapped area. The ridge appears to be broken near the position of the nova. The orientation of the emission at RA offsets from $500''$ to the west-most edge of the map is close to horizontal. At larger offsets towards the east, the ridge turns southeast. This southeastern part is also the brightest fragment of the mapped filament. It very likely continues beyond the mapped region. Most of the emission belongs to the same kinematic structure within $1.3\text{--}4.5 \text{ km s}^{-1}$. However, the channel maps in Fig. 6 show weak emission near offsets ($500''$, $50''$) at higher velocities, $5.0\text{--}7.7 \text{ km s}^{-1}$, thus revealing another overlapping cloud. The main ridge has a small velocity gradient, with velocity increasing from east to west. Only near 3.6 km s^{-1} , very weak emission is seen close to the position of the nova.

Our CO maps cover an area that is larger than the map of Scott et al. (1994) but smaller than that of Hessman (1989). The sampling, resolution, and sensitivities of our maps are far supe-

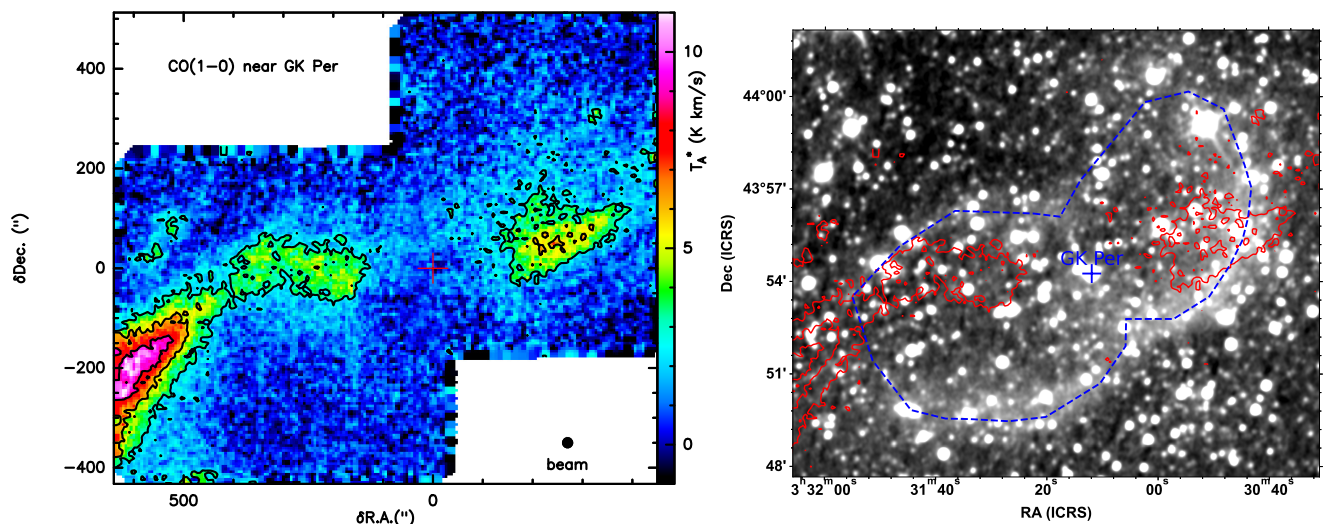


Fig. 5. Total-intensity emission of CO(1–0) near GK Per. The cross marks the position of the nova. Contours are at 3, 6, 9 times the rms noise level. Left: Color map of the CO emission. Right: The same CO contours are plotted as red solid lines over the W2 image of the field (cf. Fig. 4). The CO emission does not follow the dust emission seen in the W2 image.

rior to the earlier studies and show the region in a greater detail. It is clear that the incomplete coverage of the field in the maps of Scott et al. (1994) lead them to believe that they saw a point-symmetric structure originating from GK Per. Our maps reveal that the emission they found is only a fragment of a longer ridge that most likely is much larger than the field covered by our map and is part of the large-scale complex mapped by Hessman.

The ratio of the main-beam intensities of the CO(1–0) to (2–1) emission integrated over the entire line profile is between around 1.2 and 1.5 over most of the ridge surface, with the lower values representing the brightest southeastern part. The varying ratio reflects temperature changes coupled with variations in the line optical depth. Without measurements in one extra transition, neither can be unambiguously determined. Under the assumption of the local-thermodynamic equilibrium, however, we calculate that the typical excitation temperature is of about 12 K. Near the region with peak emission, southeast of GK Per, the CO column densities are about $1.0 \times 10^{16} \text{ cm}^{-2}$ and optical depths are about 3 or lower. In the brightest patch west of the star, the column densities are about three times lower. If the emission arises in a diffuse medium of low density, CO may be subthermally excited and a non-LTE approach would necessary for column density determinations. More transitions of CO or extra measurements in ^{13}CO would constrain the physical conditions better. We did not manage to measure ^{13}CO emission, but Hessman found a ^{12}CO to ^{13}CO emission ratio of 15 south of the area mapped by us, where the emission is stronger and more optically thick. This ratio is thus consistent with the interstellar nature of the emitting medium.

3.4. Interpretation

The mapped CO cloud has every characteristic of an interstellar translucent cloud (cf. Snow & McCall 2006). The mass of the molecular material seen in our maps can be estimated using the X-factor method. We use the X_{CO} value of 2.0×10^{20} derived for translucent clouds (Magnani & Onello 1995). Within 5σ contours of the total intensity maps of CO(1–0), which includes the western and eastern parts of the ridge, we measured an average intensity of 4.9 K km s^{-1} (in T_{mb}) and an area of $4.1 \cdot 10^4 \text{ arcsec}^2$ or $1.8 \cdot 10^{36} \text{ cm}^2$ (at 442 pc). This yields $1.8 \cdot 10^{57}$ particles of hy-

drogen or a mass of $3 M_{\odot}$. As we conservatively included only emission above 5σ , this is only a lower limit on the mass. The entire complex mapped by Hessman must be several times more massive still. Such a massive complex could not originate from the low mass cataclysmic binary GK Per.

The narrow lines that we observe in the field of GK Per are very typical for the low-density interstellar medium and would be highly unusual for any circumstellar envelope, practically ruling out the latter interpretation. As shown in Fig. 6, the peak velocities almost do not change over the different parts of the filament. For a circumstellar outflow, this would only be possible if the filamentary cloud were flowing out of the system in exactly the sky plane, which is highly unlikely (as even then a non-zero opening angle would lead to some spread in velocity). The kinematics of the molecular region is fully consistent with a quiescent interstellar cloud.

The distribution of CO emission does not correlate strongly with that of the dust emission seen in W3 and W4 maps, or with the emission of H I (Seaquist et al. 1989). A strong correlation between the three phases is not expected for the low-density ISM (e.g., Planck Collaboration et al. 2011; Reach et al. 2015). For instance, for the translucent cloud responsible for the light echoes of V838 Mon no such strong correlation is found either (see discussion in Kamiński et al. 2011).

What is then the relative location of the interstellar molecular cloud relative to GK Per? Already Hessman (1989) noticed that the harsh radiation of the nova remnant, including the dwarf nova outbursts, may photodissociate the local interstellar clouds out to a radius of 0.5 pc or 3'. Were the gap in the filament that appears to be centered on GK Per not coincidental but caused by the nova radiation, the interstellar filament must be physically close to the nova system. This would be also consistent with the 1901 light echo arising in the dusty counterpart of the CO cloud. Since forward scattering is dominating the echo generation, the scattering cloud is likely located slightly closer to us than GK Per. As noted by earlier authors, observing an evolved object such as GK Per close to an interstellar cloud is rather unexpected and should be rare. On the other hand, a few such cases are known, including the cepheid RS Pup (Kervella et al. 2012) or V732 Sgr (Sect. 2.5.1).

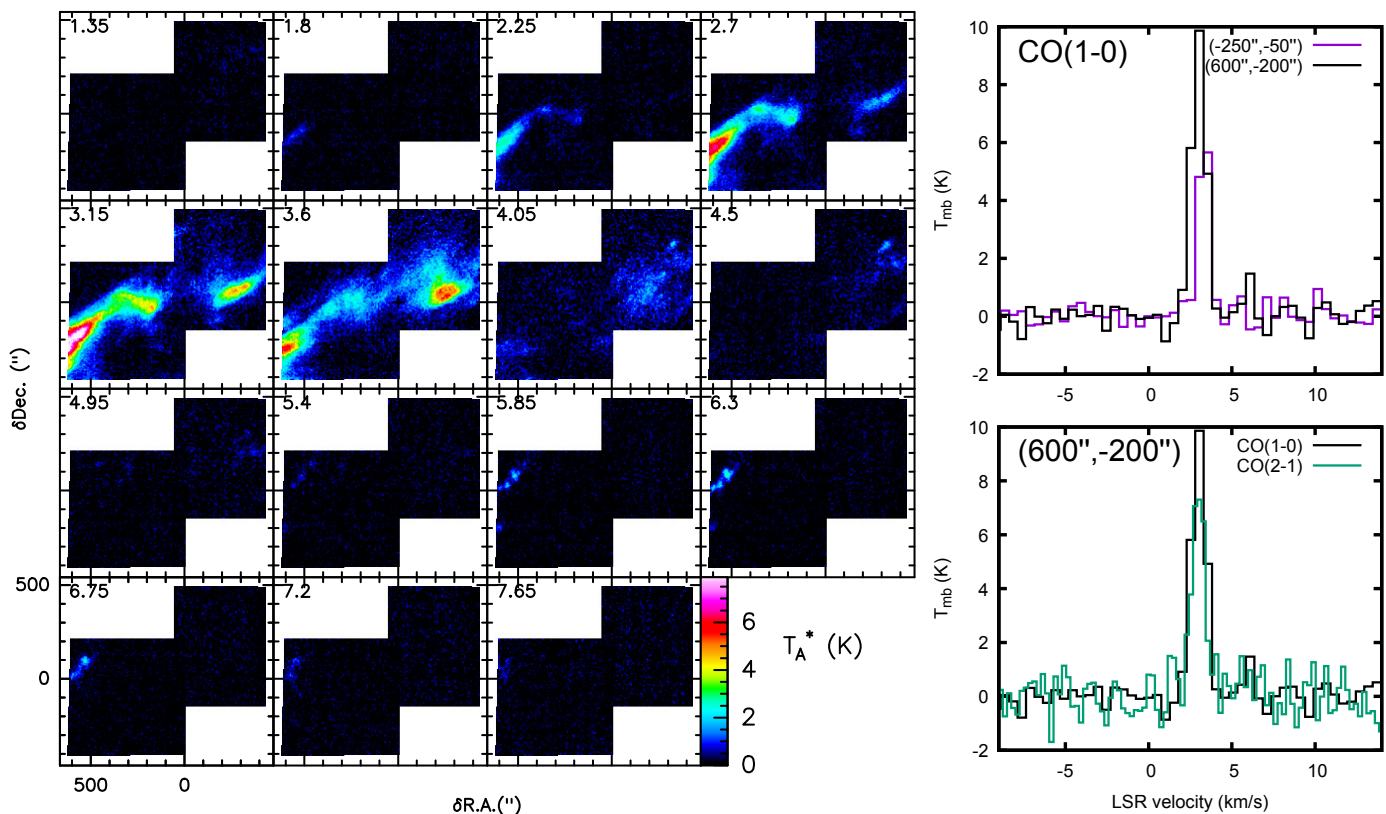


Fig. 6. Left: Channel maps of CO(1–0). The map LSR velocity is given in the upper left corner of each panel. GK Per is located at the offset of (0, 0). The maps show two clouds at 1.8–4.95 km s^{−1} and 5.4–7.65 km s^{−1}. Right: Representative spectra. Top panel compares profiles of CO(1–0) at two positions east and west of GK Per as indicated in the legend. Hardly any shift is seen, unlike ones expected for any circumstellar material. Bottom panel: Line profiles of the two lowest CO transitions are compared for the eastern position where emission is the strongest.

The systemic heliocentric velocity of GK Per is 32 (28–41) km s^{−1} (Álvarez-Hernández et al. 2021, and references therein) or 24 km s^{−1} in the LSR frame. This velocity is quite different from that of the observed CO emission in the field (1.5–8 km s^{−1}). If these velocities are used as distance indicators, the two objects could be considered as located far apart along the line of sight. On the other hand, GK Per may be moving through the local interstellar medium with a velocity that does not follow closely the overall Galactic rotation pattern. If physically related with the cloud, GK Per would have a relative radial velocity of ≈ 15 km s^{−1} (plus unknown relative tangential motion) which is supersonic and sufficient to produce a shock. Based on the proper motion of the nova, Bode et al. (2004) found a space velocity (proper and radial combined) of 45 km s^{−1}. As was noticed by Bode et al. (2004), the bipolar nebula bears some signatures of interactions with the interstellar medium, but we find no other evidence of strong interaction with the ISM.

The bipolar planetary nebula seen in WISE maps and in optical emission lines is most likely circumstellar in origin. As we have shown, it does not possess a molecular component, which is common among genuine PNe of various types and ages (e.g. Bublitz et al. 2019; Guzman-Ramirez et al. 2018). The material filling the bipolar shell may be interacting with the inner nova ejecta, as suggest in earlier studies (e.g., Harvey et al. 2016). In particular, the jet identified within the ejecta is directed near the plane of the equatorial waist of the WISE structure.

In conclusion, near GK Per we find only CO emission associated with the surrounding ISM. Elucidating the nature of the bipolar (planetary) nebula associated with GK Per is very important for understanding the full evolution of this rather bizarre

cataclysmic system. It is thus very unfortunate that it cannot be studied through mm-wave molecular lines.

4. Interferometric search of molecules in novae

It appears that all single-dish observations of classical novae have resulted in non-detections of molecular gas. This may be a consequence of insufficient sensitivities or problematic baselines. Millimeter-wave interferometric arrays are usually more sensitive and offer flat spectroscopic baselines, and thus provide the most optimal way to test classical novae for the presence of molecules (Sect. 1). Here, we present a few experiments targeting classical novae that were conducted with modern interferometric millimeter arrays.

A dedicated search for CO and HCN emission in four classical novae, NQ Vul, LW Ser, V2676 Oph, and V3662 Oph, was performed with the Submillimeter Array (SMA). We used the SWARM correlator (Primiani et al. 2016) which effectively covered four spectral ranges 224.5–232.5, 240.5–248.5, 336.0–344.0, and 352.0–360.0 GHz. The spectra thus cover the CO(2–1) transition at 230.538 GHz and the HCN(4–3) transition at 354.505 GHz. Each source was observed interchangeably with two nearby quasars, whose observations were later used for phase calibration. In each observing run, a bright quasar or a planet were observed for bandpass and absolute-flux calibration. The SMA data were calibrated in MIR⁷ and further processed (including data flagging and imaging) in CASA. We typically

⁷ <https://lweb.cfa.harvard.edu/rtdc/SMAdataprocess/mir/>

observed with 7–8 SMA antennas and at baselines from 9 to 77 m. The details and results of these observations are listed in Table 8.

None of the novae observed with the SMA was detected in molecular lines. One object, V3662 Oph or Nova Oph 2017, was observed 2 months after its discovery in outburst and about a month after detection of its near-IR first-overtone band of CO (Joshi & Banerjee 2017). In SMA data, only free-free continuum was detected in the 224–249 GHz window for this nova (Kamiński & Gehrz 2017). We achieved the best sensitivity, of 9.6 mJy, in observations of V2676 Oph in the 224–249 GHz spectra. This observation is several times deeper than our best APEX observations in CO(3–2) at an rms noise of 2 mK or about 82 mJy.

ALMA offers the greatest sensitivity among all currently available mm-wave instruments, but, to our knowledge, no program dedicated to molecule detection in classical novae has ever been conducted with the array. In the ALMA archive, we find only two classical novae observed so far. Observations towards T Pyx (L. Schmidtobreick) were obtained with the ALMA Compact Array (ACA), that is, with a smaller subset of the ALMA array composed of 7 m antennas. The observations were made in bands 4, 6, and 7, which covered several transitions commonly observed in circumstellar media, but our inspection of the available data show that no line was detected. For instance, near the SiO(3–2) line at 130.3 GHz, we get an rms of 4.0 mJy per beam of $12''.3 \times 7''.1$ and per 30 km s^{-1} . This is comparable to the sensitivity of our experiments at the SMA (given the smaller SMA beams).

The main array of ALMA observed V5668 Sgr (Nova Sgr 2015 b) in 2017 (PI: M. Diaz) in band 6. Emission in continuum and in H30 α near 231.9 GHz was reported by Diaz et al. (2018). Although their data cover CO(2–1), no molecular features were found. In a spectrum extracted for the entire continuum source of a diameter of about $0''.5$, the 3σ upper limit on the CO emission is 0.54 mJy. This is possibly the most stringent upper limit on CO emission in a classical nova to date.

The experiments to detect molecules in classical novae with mm-wave interferometers conducted for young and old novae have given negative results so far, but the number of observed sources is still small. Future similar experiments are encouraged.

5. Summary and conclusions

Our single-dish survey of the 94 old classical novae and several dwarf novae demonstrates that circumstellar envelopes of post-novae systems are poor in molecular gas. Radiation of the classical novae outburst and the interstellar radiation field must effectively destroy most molecules. Dust shielding, even if provided shortly after the eruption, must be insufficient in the later expansion phases of the nova ejecta.

With new maps of CO emission near GK Per, we debunked the long-standing conviction that the remnant of Nova 1901 is associated with a circumstellar molecular cloud. We find only interstellar emission in the direction of the nova. It is possible that the dwarf nova flashes of GK Per destroy molecules in the local ISM, reinforcing our conclusion of a deadly effect of novae on molecular material.

The lack of molecular matter in classical and dwarf novae remnants show also the remarkable difference with the newly recognized group of eruptive variables of red novae, which are rich in molecules decades and centuries after their eruptions. While red nova outbursts are often practically indistinguishable from classical novae, the amount of molecular material produced

by these two classes of objects is drastically different and may be used for new identifications of red nova in the future.

The upper limits we derive on molecular emission in classical novae are relatively shallow and do not indicate that nova shells are completely devoid of molecular matter. There is a chance that sensitive interferometric observations will be able to detect this emission, especially given the superior sensitivity of ALMA. A few experiments with the SMA and ALMA arrays have resulted in negative results so far, but the sample of novae at different times since the last eruption should be enlarged, especially for novae actively forming dust. There is still hope for measuring accurate isotopic ratios in classical novae using mm-wave data.

Acknowledgements. We thank the referee, Nye Evans, for constructive comments on the manuscript. T.K. and H.M. acknowledge funding from grant no 2018/30/E/ST9/00398 from the Polish National Science Center. R.T. acknowledge a support from grant 2017/27/B/ST9/01128 financed by the Polish National Science Center. This research has made use of the SIMBAD database, operated at CDS, Strasbourg, France. This research made use of hips2fits, <https://alaska.u-strasbg.fr/hips-image-services/hips2fits> a service provided by CDS. This paper makes use of ALMA data ADS/JAO.ALMA#2019.2.00172.S and ADS/JAO.ALMA#2016.1.00682.S. ALMA is a partnership of ESO (representing its member states), NSF (USA) and NINS (Japan), together with NRC (Canada), MOST and ASIAA (Taiwan), and KASI (Republic of Korea), in cooperation with the Republic of Chile. The Joint ALMA Observatory is operated by ESO, AUI/NRAO and NAOJ. The National Radio Astronomy Observatory is a facility of the National Science Foundation operated under cooperative agreement by Associated Universities, Inc. Based on observations with the APEX telescope under programme ID 094.F-9503(A). APEX is a collaboration between the Max-Planck-Institut für Radioastronomie, the European Southern Observatory, and the Onsala Observatory. Part of this work is based on observations carried out with the IRAM 30m telescope. IRAM is supported by INSU/CNRS (France), MPG (Germany) and IGN (Spain).

References

- Albinson, J. S. & Evans, A. 1989, MNRAS, 240, 47P
 Albinson, J. S., Evans, A., Krautter, J., & Weight, A. 1994, A&A, 284, 971
 Álvarez-Hernández, A., Torres, M. A. P., Rodríguez-Gil, P., et al. 2021, MNRAS, 507, 5805
 Amari, S., Gao, X., Nittler, L. R., et al. 2001, ApJ, 551, 1065
 Banerjee, D. P. K., Srivastava, M. K., Ashok, N. M., & Venkataraman, V. 2016, MNRAS, 455, L109
 Black, J. 2005, in High Resolution Infrared Spectroscopy in Astronomy, 3–14
 Bode, M. F. & Evans, A. 2008, Classical Novae, Vol. 43
 Bode, M. F., O’Brien, T. J., & Simpson, M. 2004, ApJ, 600, L63
 Bode, M. F., Seaquist, E. R., Frail, D. A., et al. 1987, Nature, 329, 519
 Bublitz, J., Kastner, J. H., Santander-García, M., et al. 2019, A&A, 625, A101
 Carter, M., Lazareff, B., Maier, D., et al. 2012, A&A, 538, A89
 Cox, P. & Bronfman, L. 1995, A&A, 299, 583
 Derdzinski, A. M., Metzger, B. D., & Lazzati, D. 2017, MNRAS, 469, 1314
 Diaz, M. P., Abraham, Z., Ribeiro, V. A. R. M., Beaklini, P. P. B., & Takeda, L. 2018, MNRAS, 480, L54
 Dougherty, S. M., Waters, L. B. F. M., Bode, M. F., et al. 1996, A&A, 306, 547
 Evans, A. 1997, Ap&SS, 251, 293
 Fujii, M., Arai, A., & Kawakita, H. 2021, ApJ, 907, 70
 Gehrz, R. D., Truran, J. W., Williams, R. E., & Starrfield, S. 1998, Publications of the Astronomical Society of the Pacific, 110, 3
 Güsten, R., Nyman, L. Å., Schilke, P., et al. 2006, A&A, 454, L13
 Guzman-Ramirez, L., Gómez-Ruiz, A. I., Boffin, H. M. J., et al. 2018, A&A, 618, A91
 Harvey, E., Redman, M. P., Boumis, P., & Akras, S. 2016, A&A, 595, A64
 Hessman, F. V. 1989, MNRAS, 239, 759
 Hix, W. R. 2001, Nuclear Reaction Rate Uncertainties and Their Effects on Nova Nucleosynthesis Modeling, NASA STI/Recon Technical Report N
 Howitt, G., Stevenson, S., Vigna-Gómez, A., et al. 2020a, MNRAS, 492, 3229
 Howitt, G., Stevenson, S., Vigna-Gómez, A., et al. 2020b, MNRAS, 492, 3229
 Iliadis, C., Downen, L. N., José, J., Nittler, L. R., & Starrfield, S. 2018, ApJ, 855, 76
 Izzo, L., Della Valle, M., Mason, E., et al. 2015, ApJ, 808, L14
 Joshi, V. & Banerjee, D. P. K. 2017, The Astronomer’s Telegram, 10369, 1
 Kamenetzky, J., McCray, R., Indebetouw, R., et al. 2013, ApJ, 773, L34
 Kamiński, T. & Gehrz, R. 2017, The Astronomer’s Telegram, 10536, 1
 Kamiński, T., Menten, K. M., Tyllenda, R., et al. 2015, Nature, 520, 322

Table 8. Novae observed with the SMA.

Object	Alter. name	RA (J2000)	Dec (J2000)	Obs. dates 2017	Beam _{CO} (")	Beam _{HCN} (")	rms _{CO} (mJy/beam)	rms _{HCN}
NQ Vul	Nova Vul 1976	19:29:14.75	+20:27:59.63	19,20 Jun; 5,9 Jul	3.7×3.0	3.4×2.3	13.9	15.2
LW Ser	Nova Ser 1978	17:51:50.89	-14:43:50.60	5 Jul	4.0×3.0	2.6×2.1	14.7	36.7
V2676 Oph	Nova Oph 2012	17:26:07.08	-25:51:45.40	19 Jun	4.5×3.1	2.9×2.0	9.6	27.1
V3662 Oph	Nova Oph 2017	17:39:46.08	-24:57:55.50	20 Jun	4.4×3.1	2.8×2.0	13.2	31.9

Notes. Beam sizes are given as FWHM at natural weighting of visibilities. The rms values, rms_{CO} and rms_{HCN}, are specified for a spectral bin of 30 km s⁻¹ near the rest frequencies of CO(2–1) and HCN(4–3), respectively.

- Kamiński, T., Menten, K. M., Tyllenda, R., et al. 2017, *A&A*, 607, A78
 Kamiński, T., Steffen, W., Bujarrabal, V., et al. 2021, *A&A*, 646, A1
 Kamiński, T., Steffen, W., Tyllenda, R., et al. 2018a, *A&A*, 617, A129
 Kamiński, T., Tyllenda, R., & Deguchi, S. 2011, *A&A*, 529, A48
 Kamiński, T., Tyllenda, R., Menten, K. M., et al. 2018b, *Nature Astronomy*, 2, 778
 Kato, T. & Kojiguchi, N. 2020, *PASJ*, 72, 98
 Kervella, P., Mérand, A., Szabados, L., et al. 2012, *A&A*, 541, A18
 Kimeswenger, S. 2007, in *Astronomical Society of the Pacific Conference Series*, Vol. 363, *The Nature of V838 Mon and its Light Echo*, ed. R. L. M. Corradi & U. Munari, 197
 Klein, B., Hochgürtel, S., Krämer, I., et al. 2012, *A&A*, 542, L3
 Klein, T., Ciechanowicz, M., Leinz, C., et al. 2014, *IEEE Transactions on Terahertz Science and Technology*, 4, 588
 Kochanek, C. S., Adams, S. M., & Belczynski, K. 2014, *MNRAS*, 443, 1319
 Li, F., Zhu, C., Lü, G., & Wang, Z. 2016, *Publications of the Astronomical Society of Japan*, 68 [https://academic.oup.com/pasj/article-pdf/68/3/39/6847894/psw030.pdf], 39
 Liimets, T., Corradi, R. L. M., Santander-García, M., et al. 2012, *ApJ*, 761, 34
 Loinard, L., Menten, K. M., Güsten, R., Zapata, L. A., & Rodríguez, L. F. 2012, *ApJ*, 749, L4
 Magnani, L. & Onello, J. S. 1995, *ApJ*, 443, 169
 Mayall, M. W. 1949, *AJ*, 54, R191
 Nagashima, M., Arai, A., Kajikawa, T., et al. 2014, *ApJ*, 780, L26
 Nielbock, M. & Schmidtobreick, L. 2003, *A&A*, 400, L5
 Pastorello, A., Mason, E., Taubenberger, S., et al. 2019, *A&A*, 630, A75
 Planck Collaboration, Abergel, A., Ade, P. A. R., et al. 2011, *A&A*, 536, A24
 Pontefract, M. & Rawlings, J. M. C. 2004, *MNRAS*, 347, 1294
 Primiani, R. A., Young, K. H., Young, A., et al. 2016, *Journal of Astronomical Instrumentation*, 5, 1641006
 Reach, W. T., Heiles, C., & Bernard, J.-P. 2015, *ApJ*, 811, 118
 Ritchey, G. W. 1902, *ApJ*, 15, 129
 Romano, D. & Matteucci, F. 2003, *Monthly Notices of the Royal Astronomical Society*, 342, 185
 Schaefer, B. E. 1988, *ApJ*, 327, 347
 Schaefer, B. E. 2018, *MNRAS*, 481, 3033
 Schöier, F. L., Ramstedt, S., Olofsson, H., et al. 2013, *A&A*, 550, A78
 Scott, A. D., Rawlings, J. M. C., & Evans, A. 1994, *MNRAS*, 269, 707
 Seaquist, E. R., Bode, M. F., Frail, D. A., et al. 1989, *ApJ*, 344, 805
 Shara, M. M., Zurek, D., De Marco, O., et al. 2012, *AJ*, 143, 143
 Shore, S. N. & Braine, J. 1992, *ApJ*, 392, L59
 Snow, T. P. & McCall, B. J. 2006, *ARA&A*, 44, 367
 Swope, H. H. 1940, *Harvard College Observatory Bulletin*, 913, 11
 Tweedy, R. W. 1995, *ApJ*, 438, 917
 van den Bergh, S. 1977, *PASP*, 89, 637
 Šimon, V. 2002, *A&A*, 382, 910
 Wada, Y., Yuasa, T., Nakazawa, K., et al. 2018, *MNRAS*, 474, 1564
 Warner, B. 1995, *Cataclysmic variable stars*, Vol. 28
 Weight, A., Evans, A., Albinson, J. S., & Krautter, J. 1993, *A&A*, 268, 294
 Wilson, O. C. & Merrill, P. W. 1935, *PASP*, 47, 53
 Wright, E. L., Eisenhardt, P. R. M., Mainzer, A. K., et al. 2010, *AJ*, 140, 1868
 Zwitter, T. & Munari, U. 1996, *A&AS*, 117, 449

Appendix A: Sample APEX and IRAM spectra

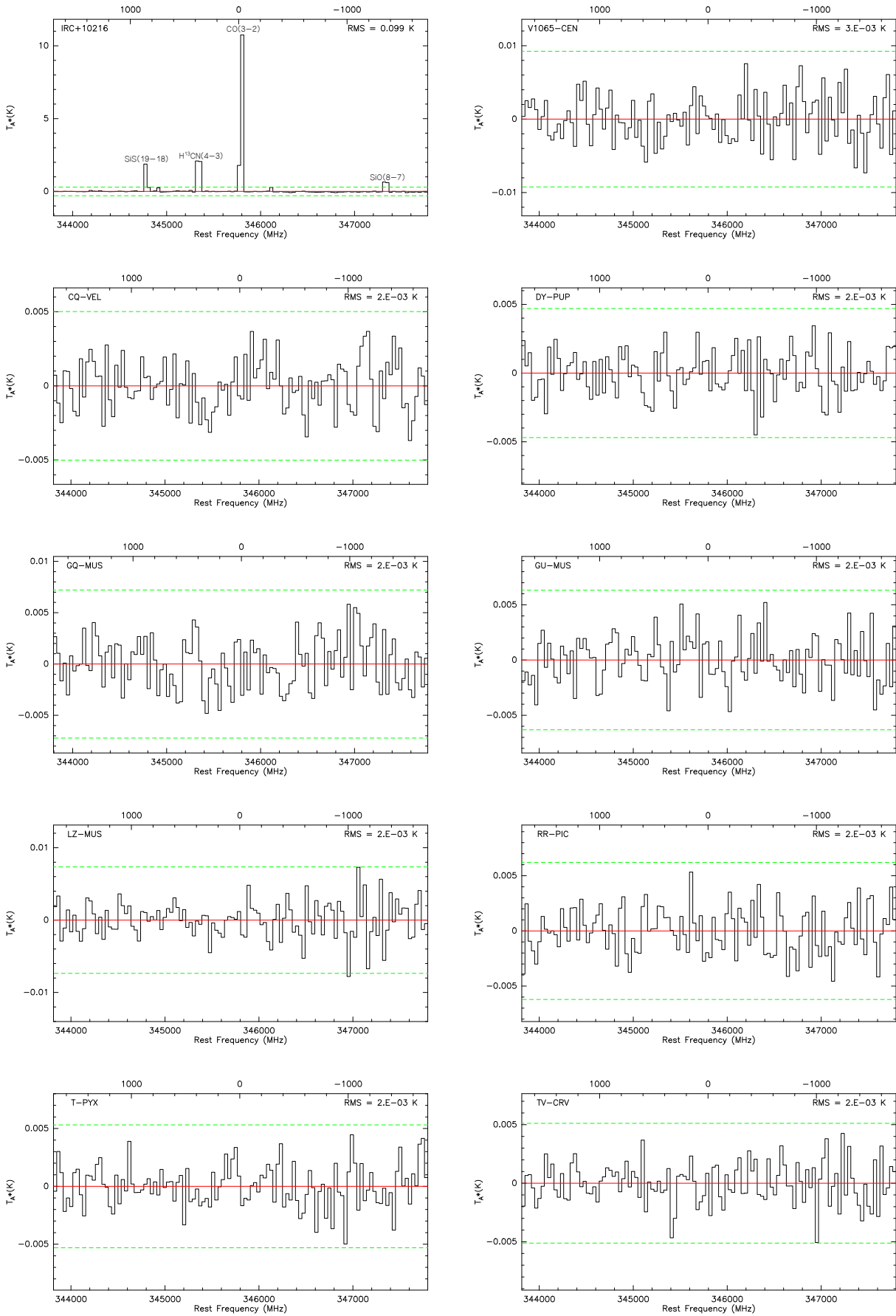


Fig. A.1. Sample spectra covering the CO(3–2) transition at a resolution of 30 km s^{-1} . The top left plot shows a reference spectrum of IRC+10216 with its most prominent lines labelled. The velocity scale is given with respect to CO(3–2). The green dashed lines mark 3σ noise levels.

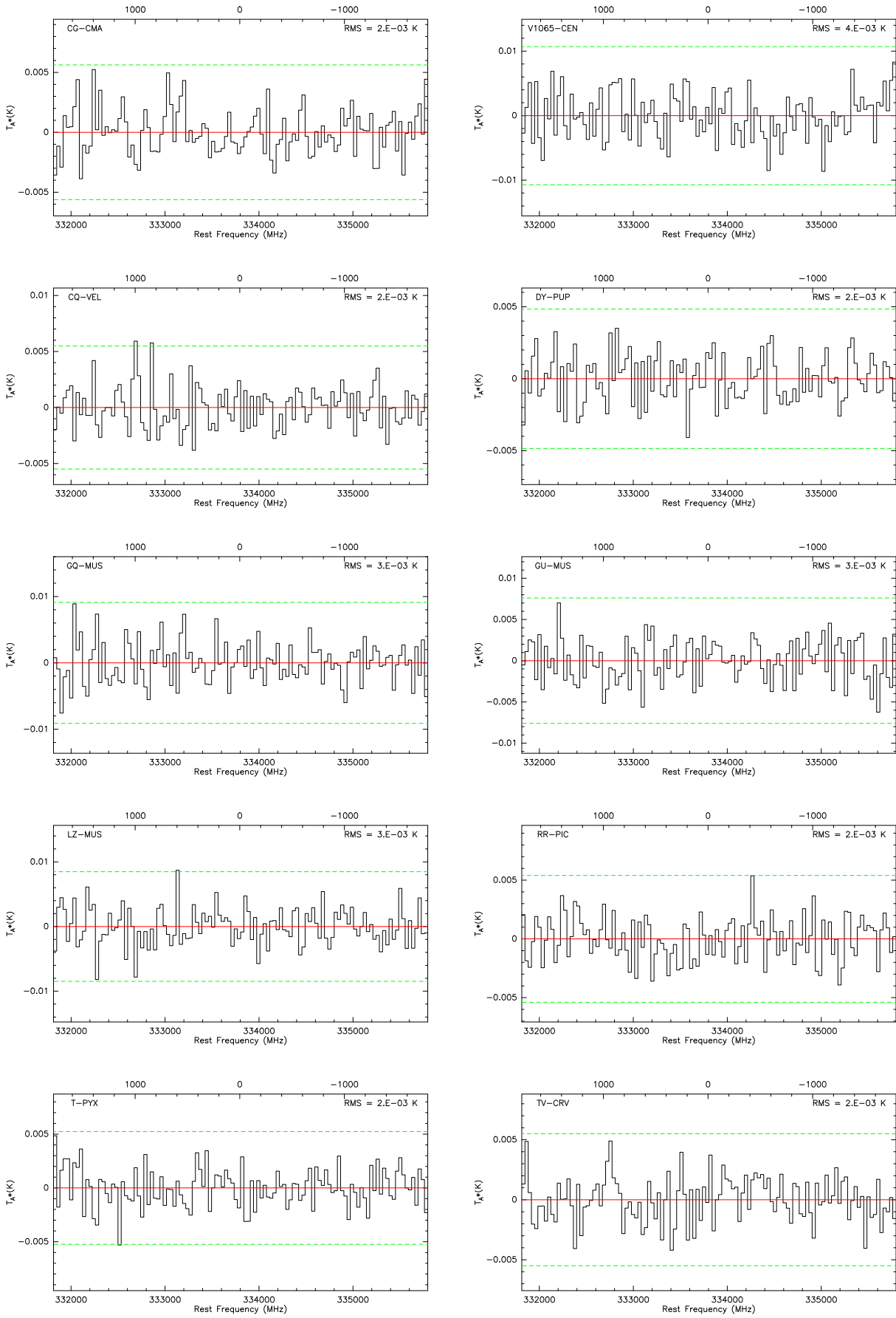


Fig. A.2. Same as Fig. A.1 but for the CO(3–2) OSB setup. The velocity scale is with respect to 333.795769 GHz.

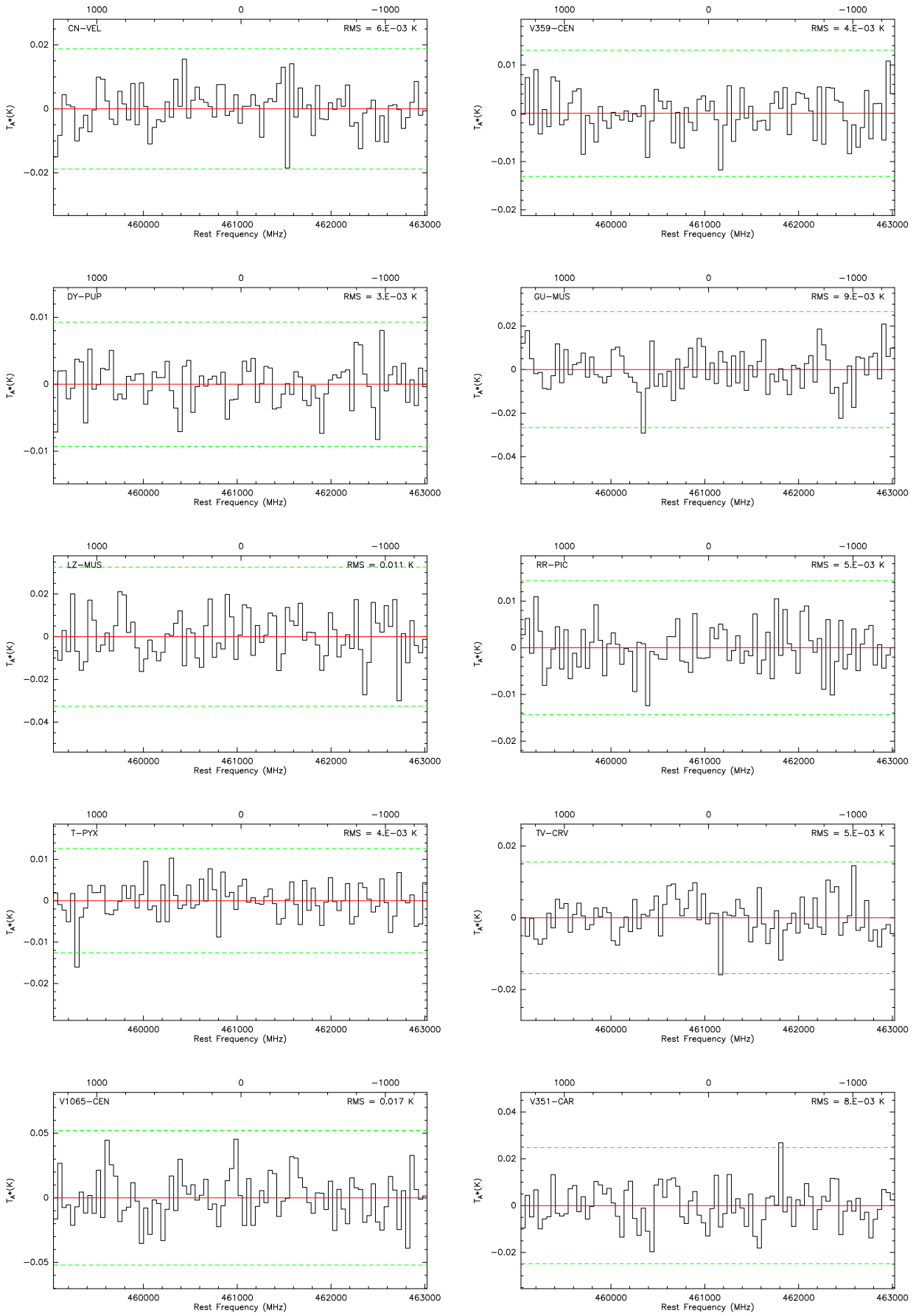


Fig. A.3. Same as Fig. A.1 but for spectra covering the CO(4-3) transition. Velocities are with respect to the rest frequency of CO(4-3).

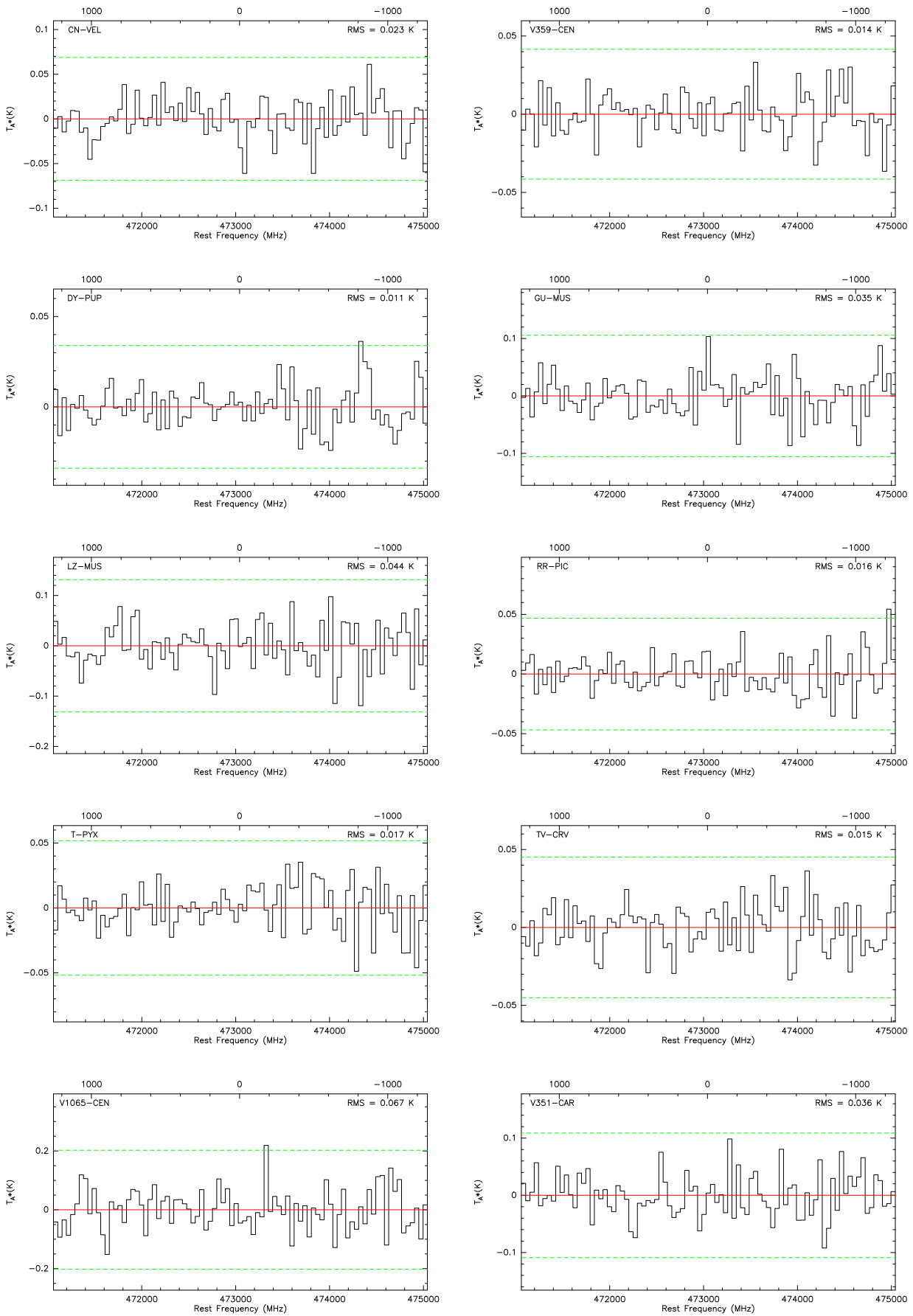


Fig. A.4. Same as Fig. A.1 but for the CO(4-3) OSB setup. The velocity scale is given relative to 473.041715 GHz.

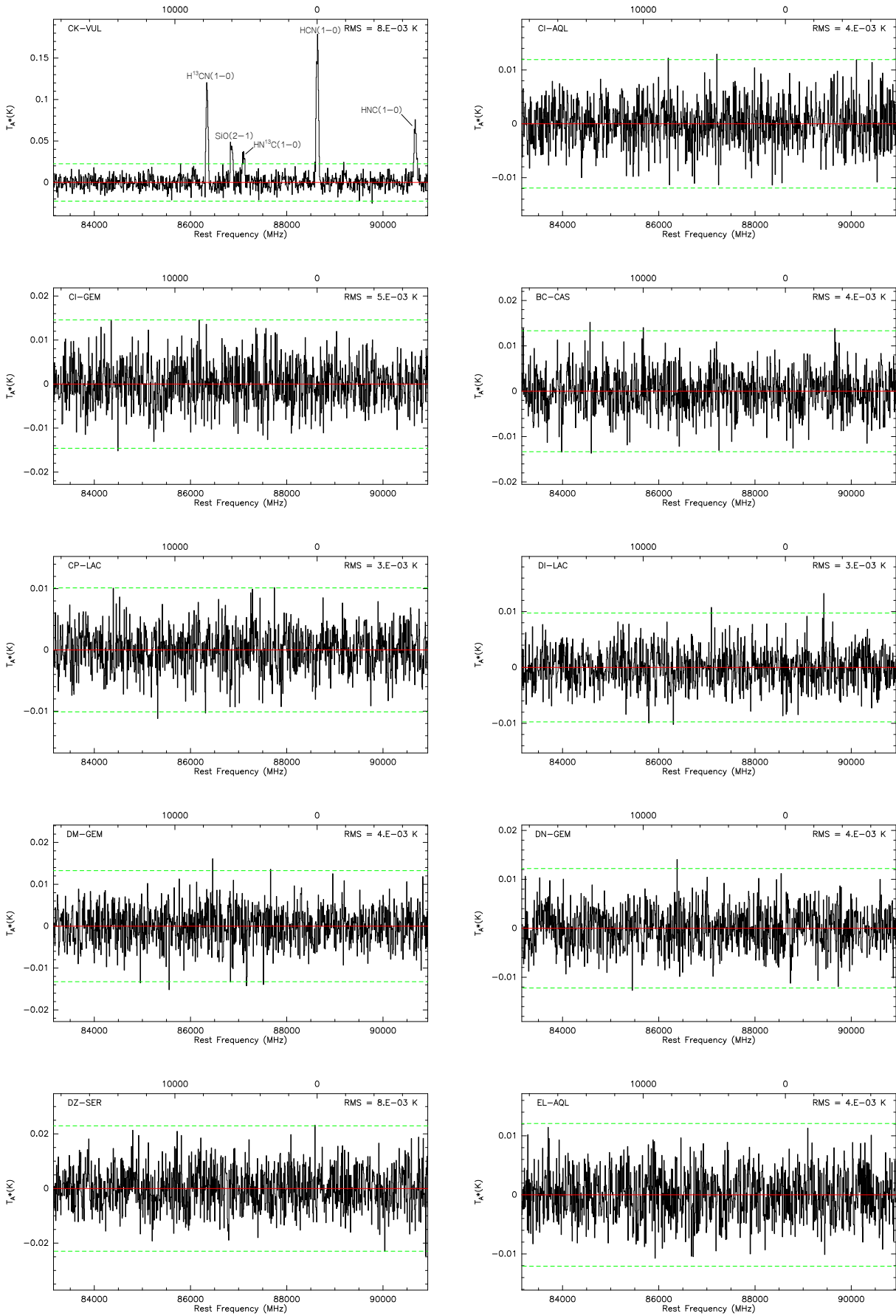


Fig. A.5. Sample IRAM/FTS spectra covering the HCN(1-0) transition and at a resolution of 30 km s^{-1} . The top left plot shows a reference spectrum of CK Vul with its most prominent lines labelled. The top axes give LSR velocity with respect to the rest frequency of HCN(1-0).

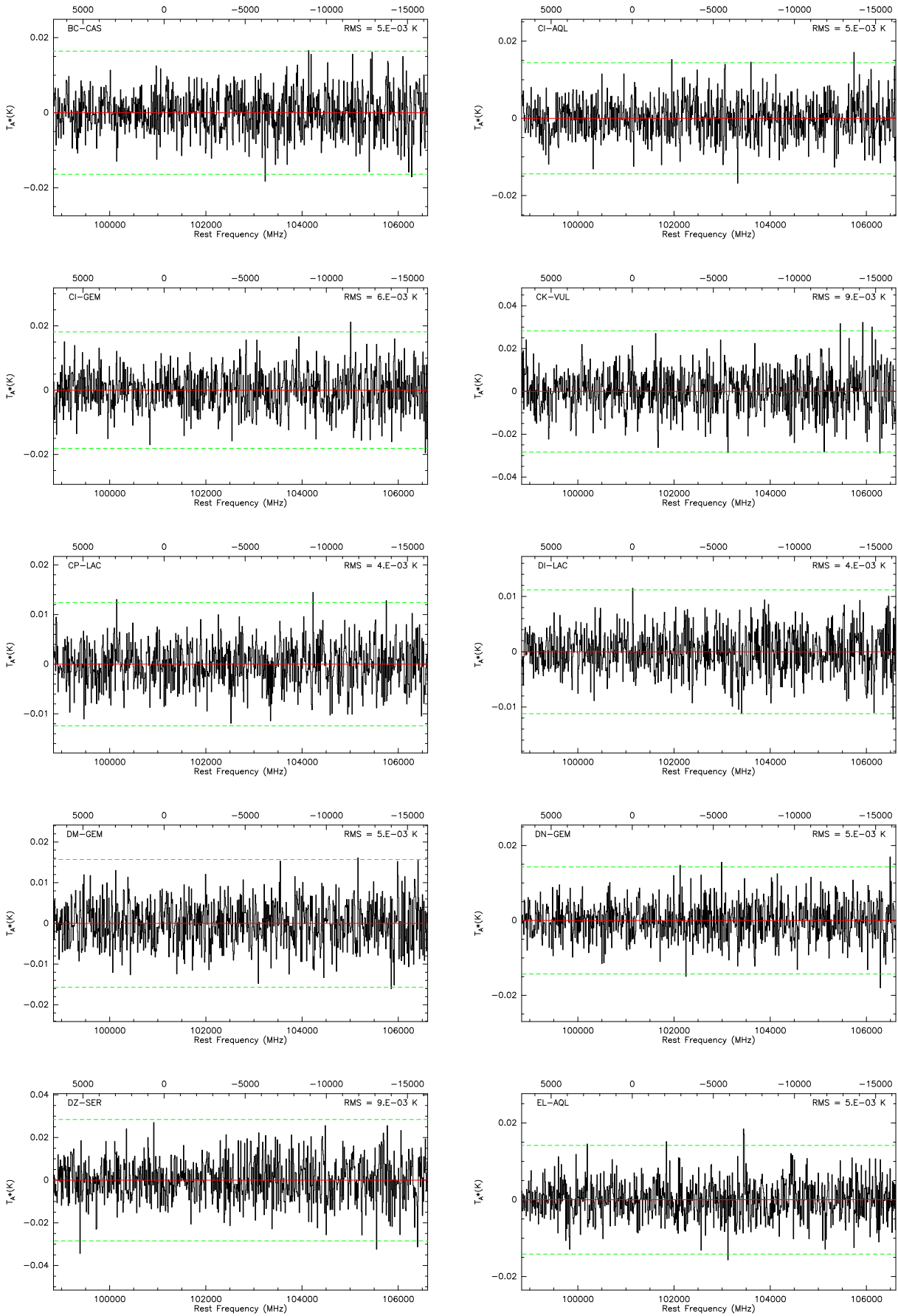


Fig. A.6. Same as Fig. A.5 but for the upper side band. The top axes give LSR velocity with respect to 101.130514 GHz.

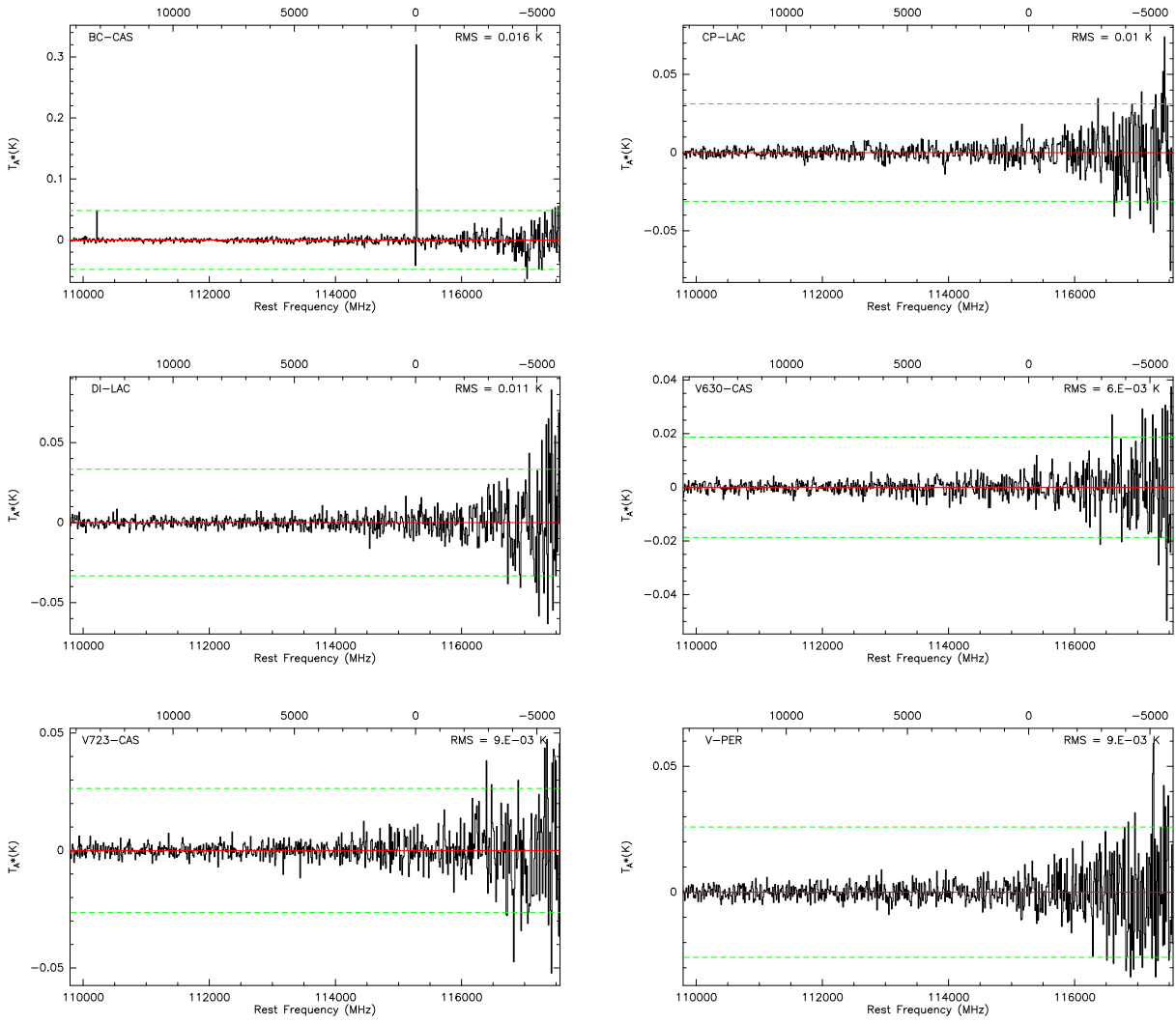


Fig. A.7. Spectra from IRAM/FTS lower side band covering the CO(1-0) transition and at a velocity resolution of 30 km s^{-1} . The velocity scale is given relative to the rest frequency of CO(1-0).

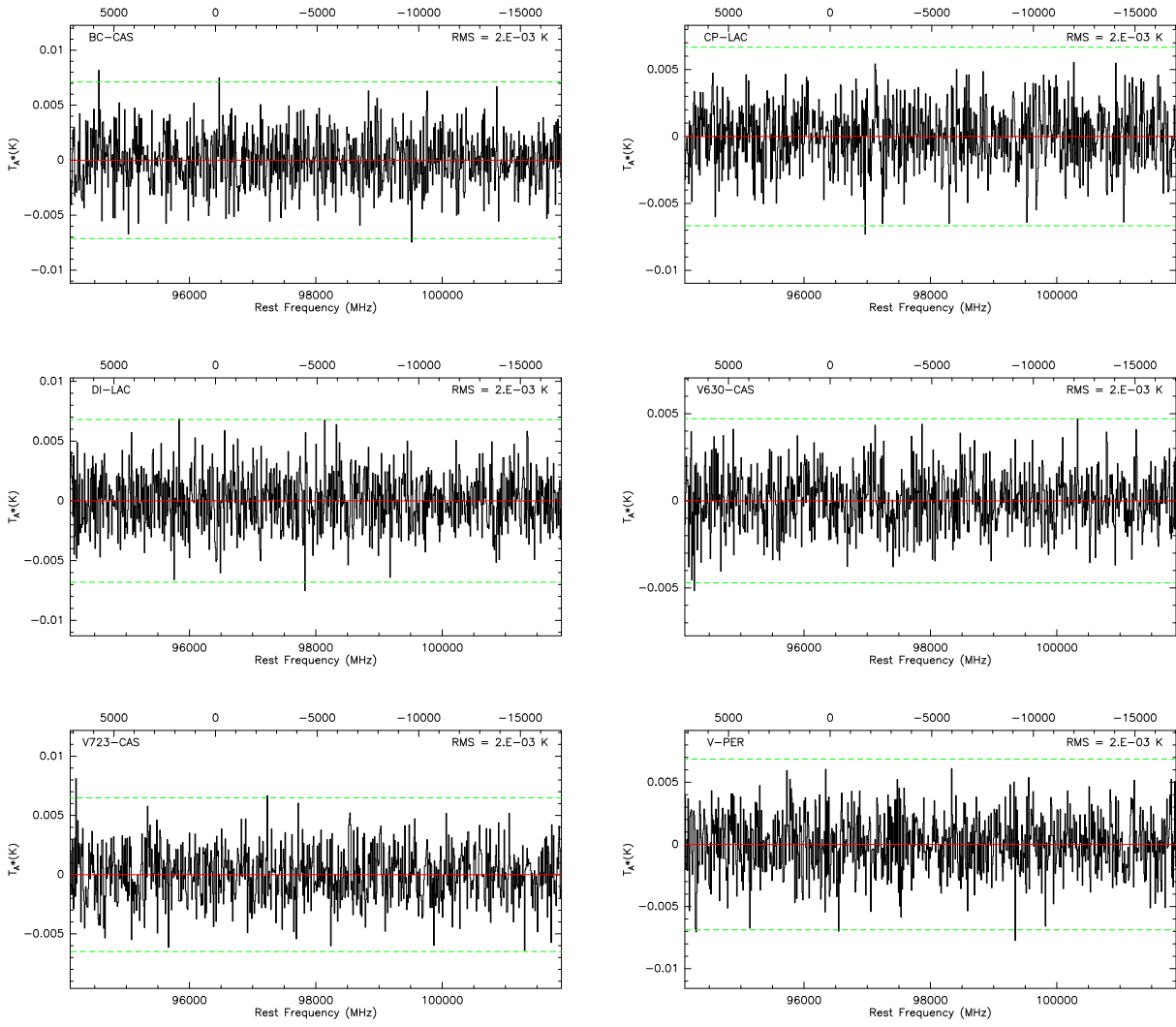


Fig. A.8. Same as Fig. A.7 but for the lower side band of the same setup. The velocity scale is relative to 96.4125766 GHz.